

Nonparametric motion control in functional connectivity studies in children with autism spectrum disorder

JIALU RAN¹, SARAH SHULTZ², BENJAMIN B. RISK¹, AND DAVID BENKESER*¹

¹ *Department of Biostatistics and Bioinformatics, Rollins School of Public Health, Emory University*

² *Department of Pediatrics, School of Medicine, Emory University*

benkeser@emory.edu

SUMMARY

Autism Spectrum Disorder (ASD) is a neurodevelopmental condition associated with difficulties with social interactions, communication, and restricted or repetitive behaviors. To characterize ASD, investigators often use functional connectivity derived from resting-state functional magnetic resonance imaging of the brain. However, participants' head motion during the scanning session can induce motion artifacts. Many studies remove scans with excessive motion, which can lead to drastic reductions in sample size and introduce selection bias. To avoid such exclusions, we propose an estimand inspired by causal inference methods that quantifies the difference in average functional connectivity in autistic and non-ASD children while standardizing motion relative to the low motion distribution in scans that pass motion quality control. We introduce a nonparametric estimator for motion control, called MoCo, that uses all participants and flexibly models the impacts of motion and other relevant features using an ensemble of machine learning methods. We establish large-sample efficiency and multiple robustness of our proposed estimator. The framework is applied to estimate the difference in functional connectivity between 132 autistic and 245 non-ASD children, of which 34 and 126 pass motion quality control. MoCo appears to dramatically reduce motion artifacts relative to no participant removal, while more efficiently utilizing participant data and accounting for possible selection biases relative to the naïve approach with participant removal.

Key words:

neuroimaging, nonparametric efficiency theory, resting-state fMRI, selection bias, stochastic intervention

1. INTRODUCTION

Early studies on neurodevelopment using functional magnetic resonance imaging found that short-range brain connections weakened and long-range brain connections strengthened during development (Fair *and others*, 2008), but these findings were undermined by the discovery that motion causes the same patterns (Van Dijk *and others*, 2012; Power *and others*, 2012; Colaço, 2024). This discovery led to the widespread adoption of motion quality control scan removal, which can result in drastic data loss. For example, multiple recent high-profile studies removed 60%-75% of approximately 11,500 children due to excessive motion (Marek *and others*, 2022; Nielsen *and others*, 2019). Removal of these children not only greatly decreases sample size, but also may introduce selection bias (Cosgrove *and others*, 2022). There is a need to develop a statistical method that makes more efficient usage of the data and avoids selection bias in order to draw unbiased inferences about brain development.

Appropriate methods for motion quality control are especially warranted in studies of neurodevelopmental conditions. Autism spectrum disorder (ASD) is a neurodevelopmental condition with a rising prevalence that affects 1 in 36 children in the United States (Maenner, 2023). To study the neurobiology of ASD, investigators often use resting-state functional magnetic resonance imaging (rs-fMRI) to derive measures of *functional connectivity* between regions in the brain. Functional connectivity is commonly defined as the correlation between the blood oxygen level dependent signal of different brain regions across time, which provides an indirect measure of neuronal activity between those regions. Disruptions of functional connectivity have been proposed as an endophenotype in autistic children (Yerys *and others*, 2015), with decades of research reporting atypical patterns of functional connectivity in diverse brain systems (Hull *and others*, 2017). However, obtaining high-quality rs-fMRI data for functional connectivity analysis is challenging. Participants' head motion during the scanning session can induce *motion artifacts*, which can bias the analysis. The patterns of correlation induced by motion artifacts mimic the connec-

tivity theory of autism, which predicts increased correlations between nearby brain regions and decreased correlations between distant brain areas (Deen and Pelphrey, 2012). Artifact-driven disruptions in brain networks can arise in comparisons of high and low motion rs-fMRI scans (Power and others, 2012).

Current guidelines for handling motion in rs-fMRI involve four steps, but the processing steps can introduce issues. First, rigid body motion correction is used to align fMRI volumes across time. Second, confound regression is applied. Several approaches to confound regression have been developed, which include regressing motion alignment parameters, global signal, cerebral spinal fluid signal, and white matter from the fMRI time courses, which may be combined with the removal of high-motion volumes or spike regression (Circic and others, 2017). However, these approaches are still insufficient, and it is recommended to remove scans in which motion is deemed unacceptable (Power and others, 2014). Nebel and others (2022) found that 80% of autistic children compared to 60% non-ASD children were removed during quality control, and the removed autistic children had greater social deficits, worse motor control, and lower generalized ability index. Fourth, the effect of diagnosis is estimated using linear regression controlling for mean framewise displacement and demographic confounders (Yan and others, 2013), where the effect is estimated using only data that pass motion quality control.

Scan removal biases and inefficiencies have been largely unaddressed in the statistical and neuroimaging literature. Nebel and others (2022) used an average-treatment effect that conditions on group in which the excluded scans are treated as missing data, which can address the selection bias issue. However, it does not utilize the outcome (resting-state correlations) in the excluded data, which may be inefficient. Additionally, it uses residuals from an initial linear regression of motion and demographic covariates restricted to the included scans, whereas a unified framework that flexibly models motion and demographic covariates has advantages. Sobel and Lindquist (2014) formulated a causal framework for task fMRI activation studies that considers the sys-

tematic error from motion, which is closely related to the nuisance regression step in resting-state fMRI preprocessing, but it does not address the problem of quality control in resting-state fMRI.

The objective of this study is to define and estimate an association between functional connectivity and ASD diagnosis that appropriately controls for the impact of motion. To this purpose, we use a causal mediation approach and consider motion as a mediator. To quantify the association between ASD and functional connectivity not related to motion, we conceptualize stochastic interventions (Muñoz and Van Der Laan, 2012) on children’s motion. Specifically, the stochastic intervention involves assigning the motion value based on a random sample from a specified distribution that corresponds to acceptable motion. By drawing children’s motion from the same acceptable motion distribution across diagnostic groups, we are able to appropriately control for the impact of motion when evaluating associations of ASD diagnosis and functional connectivity. Our approach to motion control, which we call MoCo, is a novel solution to motion artifacts that uses all participants and avoids selection bias caused by motion quality control exclusion criteria. We propose an estimator and inference based on the efficient influence function that has multiple robustness properties. Our efficient estimator utilizes a data-adaptive ensemble of machine learning algorithms to flexibly model motion and other confounders (Van der Laan and others, 2007), while retaining \sqrt{n} -consistency (Van der Laan and others, 2011). Our analysis examines functional connectivity between a seed region in the default mode network and other brain regions in children in the Autism Brain Imaging Data Exchange (Di Martino and others, 2017).

2. METHODS

Notation. Let $A \in \{0, 1\}$ denote the diagnosis group, which is equal to 1 if the participant has ASD and 0 otherwise. Let $M \in \mathcal{M}$ denote the motion variable. In our data application, we take M to be mean framewise displacement (FD), which is a commonly used measure of motion during the

resting-state fMRI scan. Let $\Delta \in \{0, 1\}$ denote an inclusion indicator, which is equal to 1 if the participant meets a pre-specified set of criteria for inclusion in the study, related to the aggregate amount of movement during a child’s scanning session. In our data application, we use the criteria from [Power and others \(2014\)](#), in which $\Delta = 1$ if a child has more than 5 minutes of data after removing frames with $\text{FD} > 0.2$ mm. Let $Y \in \mathcal{Y}$ denote the functional connectivity between two locations in the brain. For clarity, we initially define Y for a pair of regions, but in [Section 3.5](#) we will extend it to the multivariate case with family-wise error control. Let $X \in \mathcal{X}$ denote covariates that are putatively related to functional connectivity and are possibly imbalanced across diagnosis groups. Such covariates could include age, sex, and handedness. Let $Z \in \mathcal{Z}$ be variables related to the diagnosis group and the pathophysiology of ASD. These are variables that have substantially different distributions with little or no overlapping support in ASD and non-ASD groups. Such variables could include scores on the autism diagnostic observation schedule (ADOS, a measure of social disability), full-scale intelligence quotient (FIQ) score, and current medication status. The distinction between X and Z is important: X are variables that would be balanced in an ideal experiment, while Z are variables that are related to diagnosis group, and thus have distributions that depend on A .

Let $O = (A, M, \Delta, X, Z, Y)$ represent a random variable with distribution P . Denote O_1, \dots, O_n as n i.i.d. observations of O , where $O_i = (A_i, M_i, \Delta_i, X_i, Z_i, Y_i)$. We assume $P \in \mathcal{P}$, where \mathcal{P} is a statistical model for probability distributions on the support of O that is nonparametric up to certain positivity conditions that will be defined later in [Section 2.2](#).

In our notation, an uppercase letter with no subscript denotes a random variable, an uppercase letter with an index, typically i , is an observed value of a random variable, and a lowercase letter indicates a typical realization of the random variable. For example, $E(Y | A)$ is a random variable, while $E(Y | A = a)$ is a scalar.

Let $P_{M|\Delta=1,A,X}(m | a, x)$ denote the probability distribution of M conditional on $\Delta = 1, A, X$

evaluated at value $(m, a, x) \in \mathcal{M} \times \{0, 1\} \times \mathcal{X}$. $P_{M|\Delta=1,A,X}$ is thus the probability distribution of motion given fixed diagnosis status A and covariates X , among children who meet the inclusion criteria. We use $p_{M|\Delta=1,A,X}(m | a, x)$ to denote a density with respect to some dominating measure. For simplicity, we write this density and all subsequent densities as being defined with respect to the Lebesgue measure. We follow similar conventions to define $p_{M|A,X,Z}(m | a, x, z)$ as the conditional density of M given A, X, Z and $p_{Z|A,X}(z | a, x)$ as the conditional density of Z given A, X .

Let $\mu_{Y|A,M,X,Z}(a, m, x, z)$ denote the conditional mean functional connectivity given diagnosis group $A = a$, motion level $M = m$, and covariates $(X, Z) = (x, z)$. Define $\pi_a(x)$ as the conditional probability that $A = a$ given $X = x$. We use an n -subscript to denote an estimate of the corresponding estimand, e.g., $\pi_{n,a}$ is an estimate of π_a .

2.1 Defining target parameter for group comparisons in fMRI studies

We propose a framework inspired by causal mediation analysis, whereby motion is considered a mediating variable. We aim to disentangle the impact of motion in the pathway between ASD and functional connectivity. To formalize our approach, we imagine a hypothetical experiment in which we are able to manipulate the motion of children during the scanning session. The hypothetical intervention is motivated by empirical studies in which children complete training in a mock scanner (De Bie *and others*, 2010). In the data set used in our analysis, children received at least one mock training, but oftentimes this training was insufficient to adequately control motion in the scanner. Therefore, we consider defining counterfactuals based on the hypothetical intervention that could be given to children prior to scanning that would successfully reduce motion during the scan. The hypothetical training program is applied to all children irrespective of diagnosis category. Our methods mathematically formalize the nature of the training program in terms of its impact on scanner motion, define the counterfactual data that would be observed un-

der the hypothetical training program, describe assumptions under which inference can be made pertaining to the counterfactual data, and provide estimators of associations between diagnosis and functional connectivity that appropriately account for motion artifacts.

We first define the *total association* between ASD diagnosis and functional connectivity as $\theta_{O,1} - \theta_{O,0}$, where $\theta_{O,a} = E(E(Y | A = a, X))$, where the outer expectation is with respect to P_X , the marginal distribution of X . The total association can be interpreted as the mean difference functional connectivity between diagnosis groups after balancing measured confounders X and making *no effort* to control for motion. If X were balanced across diagnosis groups, i.e., if $X \perp\!\!\!\perp A$, then $\theta_{O,1} - \theta_{O,0} = E(Y | A = 1) - E(Y | A = 0)$. Therefore, the total association is adjusting for differences in the distribution of X across diagnosis groups, but nothing else. The subscript O denotes that this is an association in the *observed* data distribution that may include potentially inappropriate and imbalanced levels of motion.

Using a mediation-inspired approach, we then aim to isolate the associations of biological interest between ASD and functional connectivity from the total association by mitigating the influences of motion differences between diagnosis groups. This association of biological interest, which we term a *motion-controlled association* (MoCo), is an analogue to the classic direct effect in the causal mediation literature (Pearl, 2014). However, in this case, we do not view ASD as something that is inherently manipulable, so we restrict the interpretation of our analysis to describing direct *associations* of ASD with functional connectivity. On the other hand, we can view motion as something that *is* inherently manipulable.

We imagine a hypothetical training program where all children receive scanner training that results in a reduction of the motion of all children to a tolerable level, such that their data can be included in our analysis. The ideal motion distribution may be one where there is no motion whatsoever during a scanning session. However, such a choice is not practical since in the experimental data all children have at least *some* motion during a scanning session. Therefore,

as a practical alternative, we suggest using an estimand inspired by a *stochastic intervention* on motion. In causal inference, *static interventions* imagine counterfactual scenarios wherein a variable is set to the same fixed value for everyone. On the other hand, a stochastic intervention is one in which the value of a variable is drawn at random from a user-specified distribution (Díaz and others, 2021). We define an *acceptable motion distribution* and imagine a counterfactual scenario where all children, irrespective of diagnosis category, receive sufficient training such that the distribution of motion that would be observed in the counterfactual scenario corresponds to this acceptable motion distribution. The acceptable motion distribution may be allowed to depend on covariates and should be selected to represent a distribution of motion that, if present in the experimental data, would still yield biologically meaningful readouts of functional connectivity.

One choice is to use $P_{M|\Delta=1,X}(\cdot | x)$ to generate the motion value for a child with covariates x . However, in our application, the distribution of motion in children that pass motion quality control differs between diagnostic groups (Figure 1). We observe that non-ASD children that pass quality control will generally only move within a tolerable level during a scanning session, such that we can still recover biologically meaningful signals from the resulting data. Thus, we suggest using $P_{M|\Delta=1,A,X}(\cdot | 0, x)$ as the acceptable distribution of motion. Let $M_0 \sim P_{M|\Delta=1,A,X}(m | 0, x)$ be the counterfactual motion that would be observed for a child in the counterfactual scenario under our stochastic intervention.

Let $Y(M_0)$ denote the counterfactual functional connectivity that would be measured under this training provided in our hypothetical experiment. The counterfactual data unit generated in this scenario is $O_C = (A, M_0, X, Z, Y(M_0)) \sim P_C$, where the probability distribution of evaluated at an observation $o_c = (a, m_0, x, z, y)$ can be written $P_C(o_c) = P_{C,Y(M_0)|A,M,X,Z}(y | a, m_0, x, z)P_{M|\Delta=1,A,X}(m_0 | 0, x)P_{Z|A,X}(z | a, x)P_X(x)$. The scanner training program in our hypothetical experiment leads to a motion distribution under P_C that is described by $P_{M|\Delta=1,A,X}(\cdot | 0, x)$ as opposed to the motion distribution $P_{M|A,X,Z}(\cdot | a, x, z)$ observed in the real experiment.

The counterfactual motion is conditionally independent of diagnostic group (A) and diagnosis-specific variables (Z) given demographic covariates (X), which is consistent with our goal to control for the impact of motion in the two groups. Similarly, the conditional distribution of measured functional connectivity $Y(M_0)$ may be altered under P_C relative to the measured functional connectivity Y under P .

Using this counterfactual construction, we can then define a motion-controlled association $\theta_{C,1} - \theta_{C,0}$, where $\theta_{C,a} = E\{E_C[Y(M_0) \mid A = a, X]\}$, and we use E_C to denote expectation under P_C and the subscript C to denote that this is an association defined with respect to a counterfactual distribution. The motion-controlled association provides a comparison of the ASD and non-ASD group that controls for (i) X differences between diagnosis groups (as with the total association); *and additionally* (ii) differences in motion between the two diagnosis groups by ensuring that the X -conditional motion distribution is the same across diagnosis groups.

2.2 Identifying the motion-controlled association of ASD and brain connectivity

Identifiability of $\theta_{C,a}$ for $a = 0, 1$ can be established under the following assumptions:

(A1) *Positivity*: (A1.1) for every x such that $p_X(x) > 0$, we also have $\pi_a(x) > 0$ for $a = 0, 1$;

(A1.2) for every (x, z, m) such that $p_X(x)p_{Z|A,X}(z \mid a, x)p_{M|\Delta=1,A,X}(m \mid 0, x) > 0$, we also have that $p_{M|A,X,Z}(m \mid a, x, z) > 0$ for $a = 0, 1$.

(A2) *Mean exchangeability*: for all m such that $P\{p_{M|\Delta=1,A,X}(m \mid 0, X) > 0\} > 0$, $E_C\{Y(m) \mid A = a, X, Z\} = E_C\{Y(m) \mid A = a, M = m, X, Z\}$ a.e.- P .

(A3) *Causal Consistency*: for any child with observed motion value $M = m$, the observed functional connectivity measurement Y is equal to the counterfactual functional connectivity measurement $Y(m)$.

At the end of this section, we describe how our proposal yields biologically relevant inference

even when (A2) and (A3) do not hold.

Assumption (A1.1) states that, at a population level, there cannot be values of X that are observed exclusively in the ASD group or exclusively in the non-ASD group. In our application, X consists of age, sex, and handedness. These characteristics do not perfectly predict ASD and therefore assumption (A1.1) is plausible. (A1.2) stipulates that, for both ASD and non-ASD children with the same value x of X , it is possible to observe the *same range* of motion values *irrespective* of the value of Z . Recall that one of the components of Z is a measure of social disability, and we expect that children with higher support needs will move more in the scanner. This assumption requires that it is possible to obtain some low-motion data even in more challenging cases. This assumption could be scrutinized empirically by studying the distribution of an estimate of the ratio of motion distributions $r_a(M, X, Z)$ introduced in equation (3.2). We show results of such an analysis in Supplementary Material Section 7.2. The analysis indicates the positivity assumptions are plausible for the real data analysis.

Assumption (A2) implies that conditioned on X , Z , and diagnosis status A , there is no unmeasured confounding between $Y(m)$ and M . The plausibility of this assumption could be scrutinized, for example, by establishing conditional d -separation of Y and M in a graph (Richardson and Robins, 2013). However, because this assumption is fundamentally an assumption on the counterfactual distribution P_C , it cannot be fully verified empirically.

Assumption (A3) stipulates that the observed functional connectivity from children who naturally have motion level m is the same as the functional connectivity that would have been observed under our hypothetical experiment where children receive training in the scanner. This assumption would be violated, for example, if the hypothetical scanner training received by children had an impact on the underlying functional connectivity of the child’s brain. This assumption seems plausible but is not verifiable empirically.

Under these assumptions, we have the following theorem.

THEOREM 2.1 Under (A1)-(A3), the counterfactual $\theta_{C,a}$ is identified by θ_a , where

$$\theta_a = \iiint \mu_{Y|A,Z,M,X}(a, z, m, x) p_{Z|A,X}(z | a, x) p_{M|\Delta=1,A,X}(m | 0, x) p_X(x) dz dm dx.$$

The proof is in the Supplementary Material Section 1. The parameter θ_a involves integrating the conditional mean functional connectivity $\mu_{Y|A,M,X,Z}$ over the distributions of Z , M , and X in a sequential manner. We note that the integration over Z is specific to diagnosis group a , while the integration over M and X is the same irrespective of diagnosis group. Thus, a comparison of θ_1 and θ_0 provides a marginal associative measure that describes the joint impact of diagnosis category A and diagnosis-specific variables Z on functional connectivity while controlling for both motion M and covariates X .

We conclude this section by noting that inference on $\theta_1 - \theta_0$ may be biologically relevant *even in settings* where the fundamentally untestable assumptions (A2) and (A3) do not hold. To make this argument, we define

$$\eta_{\mu|A,M,X}(a, m, x) = \int \mu_{Y|A,M,X,Z}(a, m, x, z) p_{Z|A,X}(z | a, x) dz, \quad (2.1)$$

and note that $\eta_{\mu|A,M,X}(1, m, x) - \eta_{\mu|A,M,X}(0, m, x)$ describes an m - and x -specific difference in functional connectivity between diagnosis groups. Thus,

$$\theta_1 - \theta_0 = \iint \{\eta_{\mu|A,M,X}(1, m, x) - \eta_{\mu|A,M,X}(0, m, x)\} p_{M|\Delta=1,A,X}(m | 0, x) p_X(x) dm dx,$$

simply standardizes these m - and x -specific associations over the selected acceptable motion distribution and distribution of covariates, thereby controlling for motion and covariate differences between diagnostic groups. We argue that this is likely still a biologically relevant parameter for describing differences in functional connectivity between diagnosis groups even when (A2)-(A3) do not hold.

3. ESTIMATION AND INFERENCE

3.1 Efficiency theory

In this section, we develop an efficient estimator of θ_a . A key step in developing our estimator is deriving the *efficient influence function* of regular, asymptotically linear estimators of θ_a . See Supplementary Material Section 2.1 for a short review of efficiency theory. To characterize this efficient influence function, we define $\pi_{\Delta=1|A,X}(0, x) = P(\Delta = 1 \mid A = 0, X = x)$ as the probability of a non-ASD child with covariate value x having usable data. We introduce the shorthand $\bar{\pi}_0(x) = \pi_0(x)\pi_{\Delta=1|A,X}(0, x)$ as the probability that $A = 0$ and $\Delta = 1$ conditional on $X = x$. We denote the indicator function $\mathbb{1}_a(A_i)$ equal to 1 if $A_i = a$ and zero otherwise; $\mathbb{1}_{0,1}(A_i, \Delta_i)$ equal to 1 if $A_i = 0$ and $\Delta_i = 1$ and equals zero otherwise. We also define for $a = 0, 1$

$$r_a(m, x, z) = \frac{p_{M|\Delta=1,A,X}(m \mid 0, x)}{p_{M|A,X,Z}(m \mid a, x, z)}, \quad (3.2)$$

$$\eta_{\mu|A,Z,X}(a, z, x) = \int \mu_{Y|A,M,X,Z}(a, m, x, z) p_{M|\Delta=1,A,X}(m \mid 0, x) dm, \quad (3.3)$$

$$\xi_{a,\eta|X}(x) = \iint \mu_{Y|A,M,X,Z}(a, m, x, z) p_{M|\Delta=1,A,X}(m \mid 0, x) p_{Z|A,X}(z \mid a, x) dm dz. \quad (3.4)$$

In these definitions, we use a subscript notation for the functional parameters η and ξ that attempts to make explicit both the integrand in the parameter's definition, as well as the random variables that are arguments of the function. For example, the definition of $\eta_{\mu|A,Z,X}$ (3.3) involves integrating $\mu_{Y|A,M,X,Z}$, while $\eta_{\mu|A,Z,X}$ is a function of the random variables appearing in the subscript, A , Z and X . Note that Fubini's theorem allows us to write $\xi_{a,\eta|X}$ equivalently in terms of either $\eta_{\mu|A,Z,X}$ or $\eta_{\mu|A,M,X}$, $\xi_{a,\eta|X}(x) = \int \eta_{\mu|A,Z,X}(a, x, z) p_{Z|A,X}(z \mid a, x) dz = \int \eta_{\mu|A,M,X}(a, m, x) p_{M|\Delta=1,A,X}(m \mid 0, x) dm$.

THEOREM 3.1 (Efficient Influence Function). In a nonparametric model, the efficient influence

function for θ_a evaluated on a typical observation O_i is

$$\begin{aligned}
D_{P,a}(O_i) &= \frac{\mathbb{1}_a(A_i)}{\pi_a(X_i)} r_a(M_i, X_i, Z_i) \{Y_i - \mu_{Y|A,M,X,Z}(a, M_i, X_i, Z_i)\} \\
&\quad + \frac{\mathbb{1}_a(A_i)}{\pi_a(X_i)} \{\eta_{\mu|A,Z,X}(a, X_i, Z_i) - \xi_{a,\eta|X}(X_i)\} \\
&\quad + \frac{\mathbb{1}_{0,1}(A_i, \Delta_i)}{\bar{\pi}_0(X_i)} \{\eta_{\mu|A,M,X}(a, M_i, X_i) - \xi_{a,\eta|X}(X_i)\} \\
&\quad + \xi_{a,\eta|X}(X_i) - \theta_a.
\end{aligned} \tag{3.5}$$

A proof is included in the Supplementary Material Section 2.2.

We use the one-step estimation framework to define efficient estimators of θ_a (Bickel and others, 1993). Suppose we have an estimate of $\xi_{a,\eta|X}$ available, say $\xi_{n,a,\eta|X}$. An estimate of θ_a can be obtained by marginalizing $\xi_{n,a,\eta|X}$ over the empirical distribution of X , leading to an estimate of the form $\theta_{n,a} = n^{-1} \sum_{i=1}^n \xi_{n,a,\eta|X}(X_i)$. We refer to $\theta_{n,a}$ as a *plug-in estimate*. A *one-step estimator* of θ_a can be constructed as $\theta_{n,a}^+ = \theta_{n,a} + n^{-1} \sum_{i=1}^n D_{n,a}(O_i)$, where $D_{n,a}$ is an estimate of $D_{P,a}$. Thus, to construct a one-step estimate of θ_a , we require as an intermediate step estimates of the various parameters of P that appear in $D_{P,a}$. We refer to these quantities as *nuisance parameters*; they are parameters that need to be estimated as an intermediate step in the estimation of θ_a .

Examining Theorem 3.1, we find that there are several nuisance parameters that appear in $D_{P,a}$ for which we will require estimates to construct our estimate $D_{n,a}$ of $D_{P,a}$. Estimation of several of these parameters is straightforward. For example, $\mu_{Y|A,M,X,Z}$ could be estimated using mean regression of Y on A, M, X, Z . On the other hand, the η and ξ parameters involve integration and conditional densities, which generally present practical challenges in implementation. Our approach for estimation outlined below emphasizes two key points: (i) wherever possible mean regression with pseudo-outcomes is used to avoid numeric integration and conditional density estimation and (ii) flexible estimation techniques are used.

We choose to emphasize the use of mean regression because it is a technique familiar to

many applied statisticians and there are widely available tools. In our application, we focus on a flexible framework for regression, known as regression stacking or super learning (Van der Laan *and others*, 2007). Super learning is implemented by pre-specifying a so-called *library* of candidate regression estimators. Cross-validation is used to build a weighted combination of these estimators, with large sample theory indicating that the ensemble estimator will provide nuisance parameter estimates that are essentially as good or better than any of the individual candidate regression estimators considered.

Unfortunately, mean regression cannot be used exclusively in our estimation process for θ_a . We require estimates of certain conditional motion distributions described below. For this, we utilize the highly adaptive lasso, a flexible semiparametric conditional density estimator (Hejazi *and others*, 2022).

To circumvent numerical integration, we make use of a technique proposed by Díaz *and others* (2021) that re-casts these estimation problems that involve integrals and densities as an estimation problem that can be solved using mean regression with pseudo-outcomes. This technique is motivated by the fact that the definition of $\eta_{\mu|A,Z,X}(a, z, x)$ in (3.3) is equivalent to

$$\begin{aligned} & \int \mu_{Y|A,M,X,Z}(a, m, x, z) \frac{p_{M|\Delta=1,A,X}(m | 0, x)}{p_{M|\Delta=1,A,X,Z}(m | a, x, z)} p_{M|\Delta=1,A,X,Z}(m | a, x, z) dm \\ &= E \left[\mu_{Y|A,M,X,Z}(A, M, X, Z) \frac{p_{M|\Delta=1,A,X}(M | 0, X)}{p_{M|\Delta=1,A,X,Z}(M | A, X, Z)} \mid \Delta = 1, A = a, X = x, Z = z \right]. \end{aligned}$$

This equivalence suggests that $\eta_{\mu|A,Z,X}$ could be estimated using mean regression, where a pseudo-outcome $\mu_{n,Y|A,M,X,Z}(A, M, X, Z) \frac{p_{n,M|\Delta=1,A,X}(M|0,X)}{p_{n,M|\Delta=1,A,X,Z}(M|A,X,Z)}$ is regressed onto A, X , and Z using only the observations with $\Delta = 1$. In this way, we can avoid both the challenges associated with numeric integration and instead utilize super learning-based mean regression for estimation. Similar techniques involving pseudo-outcomes can be applied for the estimation of $\eta_{\mu|A,M,X}$ and $\xi_{a,\eta|X}$, as described below.

3.2 Detailed implementation

Our estimator can be implemented in the following steps.

1. *Estimate mean functional connectivity $\mu_{Y|A,M,X,Z}$.* Fit a super learner regression using functional connectivity as the outcome and including diagnosis category A , mean FD M , demographic covariates X , and diagnosis-specific covariates Z as predictors in the super learner. Using this fit, evaluate the fitted value, $\mu_{n,Y|A,M,X,Z}(a, M_i, X_i, Z_i)$ for $i = 1, \dots, n$ and for $a = 0, 1$. For a particular value of a , this can be achieved by predicting from the fitted super learner using the observed values of M, X , and Z , but replacing the observed value of A with the constant value a . Below we refer to this process as *evaluating the fitted value from the regression, setting A to a* .
2. *Estimate motion distributions $p_{M|A,X}$, $p_{M|\Delta=1,A,X}$, $p_{M|A,X,Z}$, and $p_{M|\Delta=1,A,X,Z}$.* For $p_{M|A,X}$, using the highly adaptive LASSO, estimate the conditional density of M given diagnosis A and demographic covariates X . The other three densities are estimated by further conditioning on diagnosis-specific covariates Z and/or subsetting to $\Delta = 1$. Using these fits, evaluate $p_{n,M|A,X}(M_i | a, X_i)$, $p_{n,M|\Delta=1,A,X}(M_i | a, X_i)$, $p_{n,M|A,X,Z}(M_i | a, X_i, Z_i)$, $p_{n,M|\Delta=1,A,X,Z}(M_i | a, X_i, Z_i)$ for $a = 0, 1$ and $i = 1, \dots, n$.
3. *Estimate motion-standardized functional connectivity $\eta_{\mu|A,Z,X}$ using pseudo-outcome regression.* Using estimates obtained in steps 1 and 2, for $i = 1, \dots, n$ create the pseudo-outcome $\hat{Y}_{M,i} = \mu_{n,Y|A,M,X,Z}(A_i, M_i, X_i, Z_i) \frac{p_{n,M|\Delta=1,A,X}(M_i|0,X_i)}{p_{n,M|\Delta=1,A,X,Z}(M_i|A_i,X_i,Z_i)}$. Using only observations with $\Delta_i = 1$, fit a super learner regression using \hat{Y}_M as the outcome and including diagnosis category A , diagnosis-specific covariates Z , and demographic covariates X as predictors. Evaluate the fitted value from this regression setting A to a to obtain $\eta_{n,\mu|A,Z,X}(a, Z_i, X_i)$ for $i = 1, \dots, n$.
4. *Estimate Z -standardized functional connectivity $\eta_{\mu|A,M,X}$ using pseudo-outcome regression.* Use estimates obtained in steps 1 and 2, and for $i = 1, \dots, n$ to create the pseudo-outcome $\hat{Y}_{Z,i} = \mu_{n,Y|A,M,X,Z}(A_i, M_i, X_i, Z_i) \frac{p_{n,M|A,X}(M_i|A_i,X_i)}{p_{n,M|A,X,Z}(M_i|A_i,X_i,Z_i)}$. Fit a super learner regression using \hat{Y}_Z as the outcome and including M , demographic covariates X , and diagnosis category A as predictors.

Evaluate the fitted value from this regression setting A to a to obtain $\eta_{n,\mu|A,M,X}(a, M_i, X_i)$ for $i = 1, \dots, n$.

5. *Estimate motion- and Z-standardized functional connectivity $\xi_{a,\eta|X}$.* Fit a super learner regression using $\eta_{n,\mu|A,Z,X}$ as the outcome, include diagnosis category A and demographic-specific covariates X as predictors in the super learner. For $a = 0, 1$, evaluate the fitted value from this regression setting A to a to obtain $\xi_{n,a,\eta|X}(X_i)$ for $i = 1, \dots, n$.

6. *Calculate plug-in estimate.* Define the plug-in estimate $\theta_{n,a} = n^{-1} \sum_{i=1}^n \xi_{n,a,\eta|X}(X_i)$.

7. *Estimate diagnosis distribution π_a and inclusion probability $\pi_{\Delta=1|A,X}$.* Fit a super learner regression using the diagnosis category as the outcome and including demographic covariates X as predictors. Evaluate the fitted value $\pi_{n,1}(X_i)$ for $i = 1, \dots, n$ and set $\pi_{n,0}(X_i) = 1 - \pi_{n,1}(X_i)$. Then fit an additional super learner using Δ as the outcome and including diagnosis category A and demographic covariates X as predictors in the regression. Evaluate the fitted value from this regression setting A to 0 to obtain $\pi_{n,\Delta=1|A,X}(0, X_i)$ for $i = 1, \dots, n$. Compute $\bar{\pi}_{n,0}(X_i) = \pi_{n,0}(X_i)\pi_{n,\Delta=1|A,X}(0, X_i)$ for $i = 1, \dots, n$.

8. *Evaluate estimated efficient influence function $D_{n,a}(O_i)$.* For $a = 0, 1$ and each $i = 1, \dots, n$, evaluate $D_{n,a}(O_i)$ by substituting the fitted values based on the estimated nuisance parameters obtained in steps 1-7 into equation (3.5).

9. *Compute the one-step estimator.* For $a = 0, 1$, compute $\theta_{n,a}^+ = \theta_{n,a} + n^{-1} \sum_{i=1}^n D_{n,a}(O_i)$.

3.3 Inference

Below we present two theorems establishing the consistency and asymptotic linearity, respectively, of the one-step estimator $\theta_{n,a}^+$. We define $\|\cdot\|$ to be the $L^2(P)$ norm of a given function f defined as $\|f\| = E[f(O)^2]^{1/2}$. We note that for the purposes of this definition, the function f is treated as given, even if it involves estimated quantities. Theorem 3.2 assumes the following:

(B1) *Boundedness:* $\pi_{n,a}$ is bounded below by some $\epsilon_1 > 0$, $\bar{\pi}_{n,0}$ is bounded below by some $\epsilon_2 > 0$,

and $p_{n,M|A,X,Z}(m | a, x, z)$ is bounded below by some $\epsilon_3 > 0$.

(B2) $o_p(1)$ -convergence of certain combinations of nuisance parameters: certain subsets of the nuisance parameters are consistently estimated, as described in Table 1.

	$\mu_{n,Y A,M,X,Z}$	$\eta_{n,\mu A,M,X}$	$\xi_{n,a,\eta X}$	$\bar{\pi}_{n,0}$	$\pi_{n,a}$	$p_{n,M \Delta=1,A,X}$	$p_{n,M A,X,Z}$
(B2.1)					✓	✓	✓
(B2.2)			✓			✓	✓
(B2.3)	✓	✓		✓	✓		
(B2.4)	✓				✓	✓	
(B2.5)	✓		✓			✓	

Table 1: Assumption (B2) of Theorem 3.2 (multiple robustness). Each row indicates a setting for consistency, where check marks indicate the nuisance parameters which, when they converge to true functions combined with assumptions (B1), (B3) and (B4), result in the consistency of $\theta_{n,a}^+$.

(B3) $L^2(P)$ -consistent influence function estimate: $E[\{D_{P_{\ell,a}}(O) - D_{n,a}(O)\}^2] = o_P(1)$, where $D_{P_{\ell,a}}$ denotes the in-probability limit of $D_{n,a}$ as n approaches infinity and $D_{n,a}$ is treated as a fixed function of O in this expression.

(B4) *Glivenko Cantelli influence function estimate*: the probability that $D_{n,a}$ falls in a P -Glivenko Cantelli class tends to one as $n \rightarrow \infty$.

Assumption (B1) guarantees that estimated propensities and motion densities are appropriately bounded so that the one-step estimator is never ill-defined. Assumption (B2) stipulates consistent estimations of the nuisance parameters. Assumptions (B3) and (B4) are necessary to ensure the negligibility of an empirical process term (Van Der Vaart *and others*, 1996).

THEOREM 3.2 (*Multiple robustness of the one-step estimator*). Under assumptions (B1) - (B4), $\theta_{n,a}^+ - \theta_a = o_p(1)$.

According to Theorem 3.2, our one-step estimators will only require *some* of the nuisance parameters to be consistently estimated to achieve consistency of our estimate of θ_a . For example, assumption (B2.1) implies that obtaining consistent estimates of the conditional motion densities,

$p_{M|\Delta=1,A,X}(m | 0, x)$ and $p_{M|A,X,Z}(m | a, x, z)$, and the conditional probability of ASD as a function of covariates π_a is sufficient to ensure a consistent estimator of θ_a . A proof of the theorem is in the Supplementary Material Section 3.

The following theorem characterizes the large-sample behavior of the proposed estimator.

THEOREM 3.3 (*Asymptotic linearity of the one-step estimator*). Under (B1), (B3), and

(C1) *$n^{1/2}$ -convergence of second order terms*:

$$\begin{aligned} \|\xi_{n,a,\eta|X} - \xi_{a,\eta|X}\| \|\pi_{n,a} - \pi_a\| &= o_P(n^{-1/2}), \\ \|\mu_{n,Y|A,M,X,Z} - \mu_{Y|A,M,X,Z}\| \{ &\|p_{n,M|\Delta=1,A,X}(\cdot | 0, \cdot) - p_{M|\Delta=1,A,X}(\cdot | 0, \cdot)\| \\ &+ \|p_{n,M|A,X,Z} - p_{M|A,X,Z}\|\} = o_P(n^{-1/2}), \text{ and} \\ \|p_{n,M|\Delta=1,A,X}(\cdot | 0, \cdot) - p_{M|\Delta=1,A,X}(\cdot | 0, \cdot)\| \{ &\|\eta_{n,\mu|A,M,X} - \eta_{\mu|A,M,X}\| \\ &+ \|\pi_{n,a} - \pi_a\| + \|\bar{\pi}_{n,0} - \bar{\pi}_0\|\} = o_P(n^{-1/2}). \end{aligned}$$

(C2) *Donsker influence function estimate*: the probability that $D_{n,a}$ falls in a P -Donsker class tends to one as $n \rightarrow \infty$.

then $\theta_{n,a}^+ - \theta_a = \frac{1}{n} \sum_{i=1}^n D_{P,a}(O_i) + o_P(n^{-1/2})$, and

$$n^{1/2}(\theta_{n,a}^+ - \theta_a) \Rightarrow N(0, E[D_{P,a}(O)^2]).$$

Assumption (C1) states that nuisance estimates converge to their true values at a sufficiently fast rate (so-called *quarter-rate conditions*). Assumption (C2) ensures large-sample negligibility of a certain second-order empirical process term (so-called *Donsker conditions*, [Bickel and others 1993](#)). The Donsker conditions can be eliminated through the use of cross-fitting, as described in Section 3.4. A detailed discussion of the assumptions and the proof of the theorem are in the Supplementary Material Section 4.

When all nuisance regressions are consistently estimated, $\sigma_n^2 = (n-1)^{-1} \sum_{i=1}^n \{D_{n,a}(O_i) - n^{-1} \sum_{j=1}^n D_{n,a}(O_j)\}^2$ can be used as a consistent estimate of $E[D_{P,a}(O)^2]$. Thus, an asymptoti-

cally justified $1 - \alpha$ confidence interval for θ_a may be constructed as $\theta_{n,a}^+ \pm n^{-1/2} z_{1-\alpha/2} \sigma_n$, where $z_{1-\alpha/2}$ denotes the $(1 - \alpha/2)$ -quantile of a standard Normal distribution.

By Theorem 3.3, we have $(\theta_{n,1}^+ - \theta_{n,0}^+) - (\theta_1 - \theta_0) = \frac{1}{n} \sum_{i=1}^n \{D_{P,1}(O_i) - D_{P,0}(O_i)\} + o_P(n^{-1/2})$ and the limiting distribution of $n^{1/2}\{(\theta_{n,1}^+ - \theta_{n,0}^+) - (\theta_1 - \theta_0)\}$ is $N(0, \tau^2)$, with $\tau^2 = \text{Var}(D_{P,1}(O) - D_{P,0}(O))$. The estimate $\tau_n^2 = (n - 1)^{-1} \sum_{i=1}^n \{D_{n,1}(O_i) - D_{n,0}(O_i) - n^{-1} \sum_{j=1}^n (D_{n,1}(O_j) - D_{n,0}(O_j))\}^2$ will be consistent for τ^2 under the assumptions of Theorem 3.3. Consequently, an approximate $1 - \alpha$ confidence interval for the direct association of ASD with brain connectivity in a single brain region is $(\theta_{n,1}^+ - \theta_{n,0}^+) \pm n^{-1/2} z_{1-\alpha/2} \tau_n$.

3.4 Cross-fit one-step estimation

As mentioned above, cross-fitting avoids the necessity of Donsker conditions in the proof of Theorem 3.3, which may afford us the ability to utilize more aggressive machine learning techniques as part of the super learner, while still generating well-calibrated confidence intervals and hypothesis tests. Cross-fitting can also reduce finite-sample bias and improve confidence interval coverage in some settings (Zivich and Breskin, 2021).

The cross-fitting process involves randomly dividing the data set into K parts, followed by separate cross-validation routines on each part. $K - 1$ parts of the data are used to estimate the nuisance parameters appearing in the efficient influence function using super learner with K' -fold cross-validation. In practice, we use $K = 5$ and $K' = 10$. Cross-fitting is used for all nuisance regressions and conditional density estimates. Consider the example of $\xi_{a,\eta|X}$. We denote by $\xi_{n,k,a,\eta|X}$ the estimate of $\xi_{a,\eta|X}$ obtained when the k -th part of the data is withheld from the nuisance estimation stage. Similarly, we denote by $D_{a,n,k}$ the efficient influence function evaluated at the nuisance parameters estimated without using the k -th part of the data. Denote by \mathcal{I}_k the indices of observations in the k -th part of the data and denote the number of observations in this set by n_k . The cross-fit estimate of θ_a is $\theta_{n,a}^{\text{cf}} = \frac{1}{K} \sum_{k=1}^K \left[\frac{1}{n_k} \sum_{i \in \mathcal{I}_k} \xi_{n,k,a,\eta|X}(X_i) + \frac{1}{n_k} \sum_{i \in \mathcal{I}_k} D_{a,n,k}(O_i) \right]$.

The asymptotic linearity of the cross-fit one-step estimator follows using the same arguments as in Theorem 3.3, where nuisance estimates are replaced by their k -specific counterparts and assumption (C2) is removed (van der Laan *and others*, 2011; Chernozhukov *and others*, 2018).

3.5 Simultaneous inference for associations

In order to control the family-wise error rate for tests of direct associations between ASD and brain connectivity across hundreds of regions, we conduct hypothesis testing using simultaneous confidence bands (Ruppert *and others*, 2003). Let $j = 1, \dots, J$ index the region. In our application, $J = 399$, and we use $\theta_{a,j}$ to denote the motion-controlled average functional connectivity in diagnosis group a between a seed region and region j , based on a 400-region parcellation. Similarly, we denote by $D_{P,a,j}$ the efficient influence function for diagnosis group a and region j , and by $\tau_{n,j}^2$ the region-specific estimate of the asymptotic variance. By Theorem 3.3,

$$\begin{pmatrix} \theta_{n,1,1}^+ - \theta_{n,0,1}^+ \\ \vdots \\ \theta_{n,1,J}^+ - \theta_{n,0,J}^+ \end{pmatrix} - \begin{pmatrix} \theta_{1,1} - \theta_{0,1} \\ \vdots \\ \theta_{1,J} - \theta_{0,J} \end{pmatrix} \Rightarrow N \left\{ \begin{pmatrix} 0 \\ \vdots \\ 0 \end{pmatrix}, \text{Cov} \begin{pmatrix} D_{P,1,1}(O) - D_{P,0,1}(O) \\ \vdots \\ D_{P,1,J}(O) - D_{P,0,J}(O) \end{pmatrix} \right\}, \quad (3.6)$$

where $\theta_{n,a,j}^+$ is the estimator at $A = a$ at location $j \in \{1, \dots, J\}$. An approximate $1 - \alpha$ simultaneous confidence interval is $(\theta_{n,1,1}^+ - \theta_{n,0,1}^+, \dots, \theta_{n,1,J}^+ - \theta_{n,0,J}^+)^{\top} \pm z_{\max,1-\alpha}(\tau_{n,1}, \dots, \tau_{n,J})^{\top}$, where $z_{\max,1-\alpha}$ is the $1 - \alpha$ quantile of the random variable $\max_{1 \leq j \leq J} \{n^{1/2}|(\theta_{n,1,j}^+ - \theta_{n,0,j}^+) - (\theta_{1,j} - \theta_{0,j})|/\tau_{n,j}\}$, which depends on the covariance matrix in (3.6).

To approximate $z_{\max,1-\alpha}$, Monte-Carlo integration is performed by taking 10^5 independent draws of a J -dimensional mean-zero multivariate normal random variable with covariance matrix equal to an empirical estimate of the correlation matrix derived from the covariance matrix on the right-hand side of (3.6). This correlation matrix can be estimated via the empirical correlation of the vector $(D_{n,1,1}(O) - D_{n,0,1}(O), \dots, D_{n,1,J}(O) - D_{n,0,J}(O))^{\top}$. For each of the 10^5 random draws, the maximal absolute value of the components of the vector is calculated. The critical value $z_{\max,1-\alpha}$ is approximated by calculating the empirical $(1 - \alpha)$ -quantile of these maximum values.

Wald hypothesis tests controlling family-wise error rate at level α are conducted by rejecting the null hypothesis of no association between diagnosis group and functional connectivity in the j -th region whenever $n^{1/2}|\theta_{n,1,j}^+ - \theta_{n,0,j}^+|/\tau_{n,j}$ is larger than the estimated value of $z_{\max,1-\alpha}$.

4. SIMULATION STUDY

We compared MoCo to two naïve approaches: one that mimics the removal of high-motion participants and one that does not remove any participants. We fixed the sample size to $n = 400$ and simulated covariates that are similar in distribution to the covariates in the observed data. We summarize our simulation design here, with details provided in Supplementary Material Section 5. The simulated demographic covariates X had three dimensions corresponding to sex, age, and handedness. Given covariates $X = x$, diagnosis A was drawn from a Bernoulli distribution with success probabilities defined by coefficients from logistic regression of the real data. Next, four diagnosis-specific covariates Z were generated to mimic the autism diagnostic observation schedule (ADOS), full-scale IQ (FIQ), a binary variable indicating the use of stimulant medication, and a binary variable for non-stimulants. The natural logarithm of mean FD M was generated from a normal distribution with mean defined from estimated coefficients of $A = a, X = x, Z = z$. Tolerable motion Δ was equal to 1 for $M \leq 0.2$.

We simulated the functional connectivity between a seed region equal to the default mode network and the six other parcels defined in the Yeo 7 parcellation (Yeo *and others*, 2011). We denote by Y_1, \dots, Y_6 the simulated functional connectivity for these six parcels. We simulated 1000 data sets such that the true associations between the diagnosis group and functional connectivity for parcels Y_1, \dots, Y_4 were set to zero, while Y_5 and Y_6 were simulated to have non-zero associations with diagnosis. This allowed us to evaluate both the type I error and the power. We simulated functional connectivity such that large and small negative associations existed between the diagnosis group and Y_5 and Y_6 , respectively. The data generating process also included quadratic

associations between motion and observed functional connectivity to examine the ability of super learner to account for possible non-linear relationships in the data. The covariance matrix for the multivariate normal was set equal to the covariance matrix of the errors obtained when fitting the functional connectivity using Super Learner. See Supplementary Material Section 5 for details.

We included the mean of the outcome, multivariate adaptive regression splines, LASSO, ridge regression, generalized additive models, generalized linear models (with and without interactions, and with and without forward stepwise covariate selection), random forest, and xgboost as candidate regressions in super learner (Polley *and others*, 2023). We compared MoCo to two naïve approaches. First, we calculated the sample mean difference in average functional connectivity between the ASD group and the non-ASD group and conducted a Welch’s two-sample t-test. Second, we excluded high-motion participants ($\Delta = 0$).

MoCo demonstrated advantages in terms of bias, MSE, type I error, and power (Table 2). For regions with zero associations, the bias and type I error were lower in MoCo compared to the two naïve methods for all four regions, and the MSE was lowest in three of four regions. In regions with associations, MoCo exhibited greater power and lower bias in detecting these differences compared to the naïve methods. Figure 2 illustrates the results of MoCo with cross-fitting on one simulated dataset. The true association was that children with ASD had a decreased correlation between the default mode network and two large brain regions, marked in dark green and purple, with an association of zero for other brain regions. MoCo successfully recovered one of the two true associations. However, using the naïve method with participant removal resulted in missing both regions, while using the naïve method with all data picked up false positives and failed to recover any of the regions with true associations.

In the Supplementary Material Section 6, we include an additional simulation study examining the multiple robustness property of our estimators. The simulation demonstrates that the theoretical multiple robustness result has the practical impact that bias of the estimators may

be well controlled even in settings in which some of the nuisance parameters are inconsistently estimated.

5. DATA ANALYSIS OF FUNCTIONAL CONNECTIVITY IN ASD

5.1 *Data and methods*

We conducted a functional connectivity analysis using a seed region in the default mode network to investigate selection bias and motion impacts in ASD. The default mode network is a collection of brain regions that tend to co-activate during wakeful rest, including daydreaming or mind wandering. Hypoconnectivity between anterior and posterior parts of the default mode network was previously found in the Autism Brain Imaging Data Exchange (ABIDE) dataset ([Di Martino and others, 2014](#)). The default mode network has been identified as a possible endophenotype of ASD ([Yerys and others, 2015](#)). However, hypoconnectivity in the default mode network also arises from motion artifacts ([Power and others, 2012](#)). We applied our method to resting-state fMRI data from school-age children in the ABIDE dataset ([Di Martino and others, 2014, 2017](#)). We subset to 377 scans corresponding to 8 to 13-year-old children from the Kennedy Krieger Institute (KKI) and New York University (NYU) from ABIDE I and ABIDE II (Supplement Table 5). Imaging data were preprocessed using fMRIPrep ([Esteban and others, 2019](#)) as described in Supplement Section 7. We included the following covariates: diagnosis (A); age, sex, and handedness (X); Autism Diagnostic Observation Schedule (ADOS) score, Full-scale Intelligence Quotient (FIQ) score, stimulant medication status, and non-stimulant medication status (Z); and mean FD (M). The ADOS score is a standardized assessment tool used to diagnose ASD, with higher scores indicating greater social disability. Although ASD is more prevalent in males than females ([Maenner, 2023](#)), we treated sex as a confounder (X) rather than diagnosis-specific variable (Z) because sex-specific differences in functional connectivity have been previously documented ([Shanmugan and others, 2022](#)), which could mask ASD-related differences in this cohort. Mean FD is an average

of the frame-to-frame displacement calculated from the rigid body motion correction parameters used in quality control and motion correction (Esteban *and others*, 2019; Power *and others*, 2014; Di Martino *and others*, 2014).

We calculated the average time series for regions of interest defined using Schaefer’s 400-node brain parcellation, which associates each node with the resting networks from Yeo-7 (Schaefer *and others*, 2018). We then regressed the six parameters from motion alignment, the global signal (mean signal across all voxels), white matter (WM), and cerebrospinal fluid (CSF) calculated from fMRIPrep. We used COMBAT (Yu *and others*, 2018) for site harmonization to account for three protocols. For COMBAT, “site” is a factor with three levels (NYU, KKI-8 channel, KKI-32 channel) and the following covariates: diagnosis, age, sex, handedness, ADOS score, FIQ, stimulant medication status, non-stimulant medication status, and mean FD. We calculated Fisher z-transformed correlations of every brain region with region 14 (‘17networks_LH_DefaultA_pCun.1’), which is a hub of the posterior default mode network (Pham *and others*, 2022). We defined the indicator of data usability Δ equal to one if a child had more than 5 minutes of data after removing frames with $FD > 0.2$ mm (Power *and others*, 2014). This resulted in $\Delta = 0$ for 98/132 ASD (74.2%) and 119/245 non-ASD children (48.6%).

We compared the naïve estimate with participant removal (retaining $\Delta = 1$), the naïve estimate with no participant removal, and the group difference estimated from MoCo with cross-fitting. We determined the FWER-critical values using simultaneous confidence intervals derived from the multivariate efficient influence functions (Section 3.5). For the naïve approaches, the critical values were derived from the sample correlation matrices of residuals of the regression $Y \sim A$. Nuisance regressions involved in our method are estimated using the same super learner library as the simulations. To handle Monte Carlo variability resulting from cross-validation, we generated estimates 50 times and calculated the averaged estimates and z-statistics across runs.

We examined positivity assumptions by making histograms of the inverse probability weights

and density ratios that appear in the efficient influence function (see Supplementary Material Section 7.2). Positivity issues arise if inverse weights or density ratios are very large. Assumptions appear to be adequately met, as the values of the estimated density ratios evaluated on the observed data never exceeded 4.

5.2 Results

Both MoCo and the naïve approach use data from 377 participants, including 132 with ASD, while the naïve approach with participant removal uses 160 participants, and only 34 with ASD. MoCo reveals four regions that differ in connectivity with the posterior default mode seed region in ASD versus non-ASD at FWER=0.05, including three regions of hyperconnectivity with distant frontal-parietal regions (Figure 3). The naïve approach indicates more extensive differences than MoCo, including prominent default mode hypoconnectivity in ASD in long-distance correlations. These are likely spurious differences due to motion, as long-distance correlations tend to be attenuated in high-motion participants (Satterthwaite *and others*, 2013). These possible biases are also prominent in the mean connectivity estimates (Supplement Figure 3). The naïve approach also selects some regions of hyperconnectivity in ASD with lateral regions of the frontal lobe. Overall, MoCo results are more similar to the naïve approach with participant removal, although the naïve with participant removal only identifies two regions at FWER=0.05. At FWER=0.20, MoCo selects four additional regions of hypoconnectivity with the far anterior part of the frontal lobe (plus one region of hyperconnectivity with ventral attention), but much less extensive than in the naïve approach.

6. DISCUSSION

We introduce MoCo, a method for controlling motion in fMRI studies to estimate the difference in functional connectivity between ASD and non-ASD children when all children have a tolerable

level of motion. Our theoretical framework enables the use of flexible machine-learning techniques for parameter estimation. The method allows the estimation of simultaneous confidence intervals for controlling FWER across hundreds of brain connections. It shows improved statistical power in identifying the true association and a lower type I error rate in the absence of an association. Our approach avoids selection bias caused by motion quality control exclusion criteria.

Our findings differ greatly from the naïve approach, which suggested hypoconnectivity across many DMN regions when including all participants. The naïve approach with participant removal suggests these differences were due to motion artifacts, but it is difficult to disentangle this from power loss and selection biases, as only 34 ASD children passed motion quality control. MoCo contributes to the ASD literature by flexibly modeling motion artifacts while including all the phenotypic variability in the study sample, providing stronger evidence that the hypoconnectivity differences were due to motion artifacts. MoCo recovered more regions than the naïve approach with motion removal (four versus two at FWER=0.05), although the overall picture suggests relatively minor differences between autistic and non-ASD children in this study sample.

An important decision in the modeling process is to designate variables as possible confounders X or variables related to diagnosis group Z . In the data analysis, we consider age, sex, and handedness as possible confounders X , all of which can potentially affect the associations between ASD and functional connectivity due to an imbalanced study design. We treat FIQ as a diagnosis-specific variable, which on average was lower in the ASD group. However, FIQ is highly variable in autism, and whether or not it should be considered as a possible confounder or as a diagnosis-specific variable is debatable. In our dataset, the child with the highest FIQ was also diagnosed with autism (Supplement Table 5). Neural diversity in autism is associated with strengths like unique perspectives, problem-solving skills, intense focus, attention to detail, and other traits that extend beyond a single measure of intelligence. A limitation in our data analysis is that we only considered a limited set of behavioral and diagnosis-specific covariates,

which was driven by the covariates available in the two ABIDE study sites. Additional research into the associations between functional connectivity and neural diversity may help elucidate the neurological underpinnings in ASD.

There are a number of limitations and directions for future research. Although MoCo does not exclude any children due to motion during the rs-fMRI scan, there were a few scans that failed the fMRIPrep cortical segmentation pipeline due to issues with the structural scan, and effectively have missing fMRI data (Supplement Section 7, Web Supplement Figure 1). MoCo could be extended to incorporate the behavioral and demographic information from these participants. Our study fits functional connectivity for a seed-based analysis, rather than simultaneously analyzing the functional connectivity matrix. A matrix-variate approach could be designed to exploit low-rank or sparse structure, which may improve efficiency (Wang and Guo, 2023). Additionally, we focus on rs-fMRI, but MoCo may be effective in other neuroimaging modalities. Motion tends to cause spurious cortical thinning in brain morphometry studies (Reuter *and others*, 2015) and can cause spurious group differences in diffusion MRI (Yendiki *and others*, 2014).

REFERENCES

- BICKEL, PETER J, KLAASSEN, CHRIS AJ, RITOV, YA'ACOV AND WELLNER, JON A. (1993). *Efficient and adaptive estimation for semiparametric models*, Volume 4. Springer.
- CHERNOZHUKOV, VICTOR, CHETVERIKOV, DENIS, DEMIRER, MERT, DUFLO, ESTHER, HANSEN, CHRISTIAN, NEWEY, WHITNEY AND ROBINS, JAMES. (2018). Double/debiased machine learning for treatment and structural parameters. *The Econometrics Journal* **21**(1), C1–C68.
- CIRIC, RASTKO, WOLF, DANIEL H, POWER, JONATHAN D, ROALF, DAVID R, BAUM, GRAHAM L *and others*. (2017). Benchmarking of participant-level confound regression strategies for

- the control of motion artifact in studies of functional connectivity. *Neuroimage* **154**, 174–187.
- COLAÇO, DAVID. (2024). When remediating one artifact results in another: control, confounders, and correction. *History and Philosophy of the Life Sciences* **46**(1), 5.
- COSGROVE, KELLY T, McDERMOTT, TIMOTHY J, WHITE, EVAN J, MOSCONI, MATTHEW W, THOMPSON, WESLEY K, PAULUS, MARTIN P, CARDENAS-INIGUEZ, CARLOS AND AUPPERLE, ROBIN L. (2022). Limits to the generalizability of resting-state functional magnetic resonance imaging studies of youth: An examination of abcd study® baseline data. *Brain imaging and behavior* **16**(4), 1919–1925.
- DE BIE, HENRICA MA, BOERSMA, MARIA, WATTJES, MIKE P, ADRIAANSE, SOFIE, VERMEULEN, R JEROEN *and others*. (2010). Preparing children with a mock scanner training protocol results in high quality structural and functional mri scans. *European journal of pediatrics* **169**, 1079–1085.
- DEEN, BEN AND PELPHREY, KEVIN. (2012). Perspective: brain scans need a rethink. *Nature* **491**(7422), S20–S20.
- DI MARTINO, ADRIANA, O’CONNOR, DAVID, CHEN, BOSI, ALAERTS, KAAT, ANDERSON, JEFFREY S, ASSAF *and others*. (2017). Enhancing studies of the connectome in autism using the autism brain imaging data exchange ii. *Scientific data* **4**(1), 1–15.
- DI MARTINO, ADRIANA, YAN, CHAO-GAN, LI, QINGYANG, DENIO, ERIN, CASTELLANOS *and others*. (2014). The autism brain imaging data exchange: towards a large-scale evaluation of the intrinsic brain architecture in autism. *Molecular psychiatry* **19**(6), 659–667.
- DÍAZ, IVÁN, HEJAZI, NIMA S, RUDOLPH, KARA E AND VAN DER LAAN, MARK J. (2021). Nonparametric efficient causal mediation with intermediate confounders. *Biometrika* **108**(3), 627–641.

- ESTEBAN, OSCAR, MARKIEWICZ, CHRISTOPHER J, BLAIR, ROSS W, MOODIE, CRAIG A, ISIK, A *and others*. (2019). fmriprep: a robust preprocessing pipeline for functional mri. *Nature methods* **16**(1), 111–116.
- FAIR, DAMIEN A, COHEN, ALEXANDER L, DOSENBACH, NICO UF, CHURCH, JESSICA A, MIEZIN, FRANCIS M, BARCH, DEANNA M, RAICHEL, MARCUS E, PETERSEN, STEVEN E AND SCHLAGGAR, BRADLEY L. (2008). The maturing architecture of the brain’s default network. *Proceedings of the National Academy of Sciences* **105**(10), 4028–4032.
- HEJAZI, NIMA S, VAN DER LAAN, MARK J AND BENKESER, DAVID. (2022). haldensify: Highly adaptive lasso conditional density estimation inr. *Journal of Open Source Software* **7**(77), 4522.
- HULL, JOCELYN V, DOKOVNA, LISA B, JACOKES, ZACHARY J, TORGERSON, CARINNA M, IRIMIA, ANDREI AND VAN HORN, JOHN DARRELL. (2017). Resting-state functional connectivity in autism spectrum disorders: a review. *Frontiers in psychiatry* **7**, 205.
- MAENNER, MATTHEW J. (2023). Prevalence and characteristics of autism spectrum disorder among children aged 8 years—autism and developmental disabilities monitoring network, 11 sites, united states, 2020. *MMWR. Surveillance Summaries* **72**.
- MAREK, SCOTT, TERVO-CLEMMENS, BRENDEN, CALABRO, FINNEGAN J, MONTEZ, DAVID F, KAY, BENJAMIN P *and others*. (2022). Reproducible brain-wide association studies require thousands of individuals. *Nature* **603**(7902), 654–660.
- MUÑOZ, IVÁN DÍAZ AND VAN DER LAAN, MARK. (2012). Population intervention causal effects based on stochastic interventions. *Biometrics* **68**(2), 541–549.
- NEBEL, MARY BETH, LIDSTONE, DANIEL E, WANG, LIWEI, BENKESER, DAVID, MOSTOFSKY, STEWART H AND RISK, BENJAMIN B. (2022). Accounting for motion in resting-state fmri:

- What part of the spectrum are we characterizing in autism spectrum disorder? *NeuroImage* **257**, 119296.
- NIELSEN, ASHLEY N, GREENE, DEANNA J, GRATTON, CATERINA, DOSENBACH, NICO UF, PETERSEN, STEVEN E AND SCHLAGGAR, BRADLEY L. (2019). Evaluating the prediction of brain maturity from functional connectivity after motion artifact denoising. *Cerebral Cortex* **29**(6), 2455–2469.
- PEARL, JUDEA. (2014). Interpretation and identification of causal mediation. *Psychological methods* **19**(4), 459.
- PHAM, DAMON D, MUSCHELLI, JOHN AND MEJIA, AMANDA F. (2022). ciftitools: A package for reading, writing, visualizing, and manipulating cifti files in r. *NeuroImage* **250**, 118877.
- POLLEY, ERIC, LEDELL, ERIN, KENNEDY, CHRIS AND VAN DER LAAN, MARK. (2023). *SuperLearner: Super Learner Prediction*. R package version 2.0-28.1.
- POWER, JONATHAN D, BARNES, KELLY A, SNYDER, ABRAHAM Z, SCHLAGGAR, BRADLEY L AND PETERSEN, STEVEN E. (2012). Spurious but systematic correlations in functional connectivity mri networks arise from subject motion. *Neuroimage* **59**(3), 2142–2154.
- POWER, JONATHAN D, MITRA, ANISH, LAUMANN, TIMOTHY O, SNYDER, ABRAHAM Z, SCHLAGGAR, BRADLEY L AND PETERSEN, STEVEN E. (2014). Methods to detect, characterize, and remove motion artifact in resting state fmri. *Neuroimage* **84**, 320–341.
- REUTER, MARTIN, TISDALL, M DYLAN, QURESHI, ABID, BUCKNER, RANDY L, VAN DER KOUWE, ANDRÉ JW AND FISCHL, BRUCE. (2015). Head motion during mri acquisition reduces gray matter volume and thickness estimates. *Neuroimage* **107**, 107–115.
- RICHARDSON, THOMAS S AND ROBINS, JAMES M. (2013). Single world intervention graphs (swigs): A unification of the counterfactual and graphical approaches to causality. *Center for the*

- Statistics and the Social Sciences, University of Washington Series. Working Paper* **128**(30), 2013.
- RUPPERT, DAVID, WAND, MATT P AND CARROLL, RAYMOND J. (2003). *Semiparametric regression*, Number 12. Cambridge university press.
- SATTERTHWAITE, THEODORE D, ELLIOTT, MARK A, GERRATY, RAPHAEL T, RUPAREL, KOSHA, LOUGHEAD, JAMES *and others*. (2013). An improved framework for confound regression and filtering for control of motion artifact in the preprocessing of resting-state functional connectivity data. *Neuroimage* **64**, 240–256.
- SCHAEFER, ALEXANDER, KONG, RU, GORDON, EVAN M, LAUMANN, TIMOTHY O, ZUO, XI-NIAN *and others*. (2018). Local-global parcellation of the human cerebral cortex from intrinsic functional connectivity mri. *Cerebral cortex* **28**(9), 3095–3114.
- SHANMUGAN, SHEILA, SEIDLITZ, JAKOB, CUI, ZAIXU, ADEBIMPE, AZEEZ, BASSETT, DANIELLE S *and others*. (2022). Sex differences in the functional topography of association networks in youth. *Proceedings of the National Academy of Sciences* **119**(33), e2110416119.
- SOBEL, MICHAEL E AND LINDQUIST, MARTIN A. (2014). Causal inference for fmri time series data with systematic errors of measurement in a balanced on/off study of social evaluative threat. *Journal of the American Statistical Association* **109**(507), 967–976.
- VAN DER LAAN, MARK J, POLLEY, ERIC C AND HUBBARD, ALAN E. (2007). Super learner. *Statistical applications in genetics and molecular biology* **6**(1).
- VAN DER LAAN, MARK J, ROSE, SHERRI *and others*. (2011). *Targeted learning: causal inference for observational and experimental data*, Volume 4. Springer.
- VAN DER LAAN, MARK J, ROSE, SHERRI, ZHENG, WENJING AND VAN DER LAAN, MARK J.

- (2011). Cross-validated targeted minimum-loss-based estimation. *Targeted learning: causal inference for observational and experimental data*, 459–474.
- VAN DER VAART, AAD W, WELLNER, JON A, VAN DER VAART, AAD W AND WELLNER, JON A. (1996). *Weak convergence*. Springer.
- VAN DIJK, KOENE RA, SABUNCU, MERT R AND BUCKNER, RANDY L. (2012). The influence of head motion on intrinsic functional connectivity mri. *Neuroimage* **59**(1), 431–438.
- WANG, YIKAI AND GUO, YING. (2023). Locus: A regularized blind source separation method with low-rank structure for investigating brain connectivity. *The Annals of Applied Statistics* **17**(2), 1307–1332.
- YAN, CHAO-GAN, CHEUNG, BRIAN, KELLY, CLARE, COLCOMBE, STAN, CRADDOCK, R CAMERON, DI MARTINO, ADRIANA, LI, QINGYANG, ZUO, XI-NIAN, CASTELLANOS, F XAVIER AND MILHAM, MICHAEL P. (2013). A comprehensive assessment of regional variation in the impact of head micromovements on functional connectomics. *Neuroimage* **76**, 183–201.
- YENDIKI, ANASTASIA, KOLDEWYN, KAMI, KAKUNOORI, SITA, KANWISHER, NANCY AND FISCHL, BRUCE. (2014). Spurious group differences due to head motion in a diffusion mri study. *Neuroimage* **88**, 79–90.
- YEO, BT THOMAS, KRIENEN, FENNA M, SEPULCRE, JORGE, SABUNCU, MERT R, LASHKARI, DANIAL *and others*. (2011). The organization of the human cerebral cortex estimated by intrinsic functional connectivity. *Journal of neurophysiology*.
- YERYS, BENJAMIN E, GORDON, EVAN M, ABRAMS, DANIELLE N, SATTERTHWAITE, THEODORE D, WEINBLATT, RACHEL *and others*. (2015). Default mode network segrega-

tion and social deficits in autism spectrum disorder: Evidence from non-medicated children. *NeuroImage: Clinical* **9**, 223–232.

YU, MEICHEN, LINN, KRISTIN A, COOK, PHILIP A, PHILLIPS, MARY L, MCINNIS, MELVIN, FAVA, MAURIZIO, TRIVEDI, MADHUKAR H *and others.* (2018). Statistical harmonization corrects site effects in functional connectivity measurements from multi-site fmri data. *Human brain mapping* **39**(11), 4213–4227.

ZIVICH, PAUL N AND BRESKIN, ALEXANDER. (2021). Machine learning for causal inference: on the use of cross-fit estimators. *Epidemiology (Cambridge, Mass.)* **32**(3), 393.

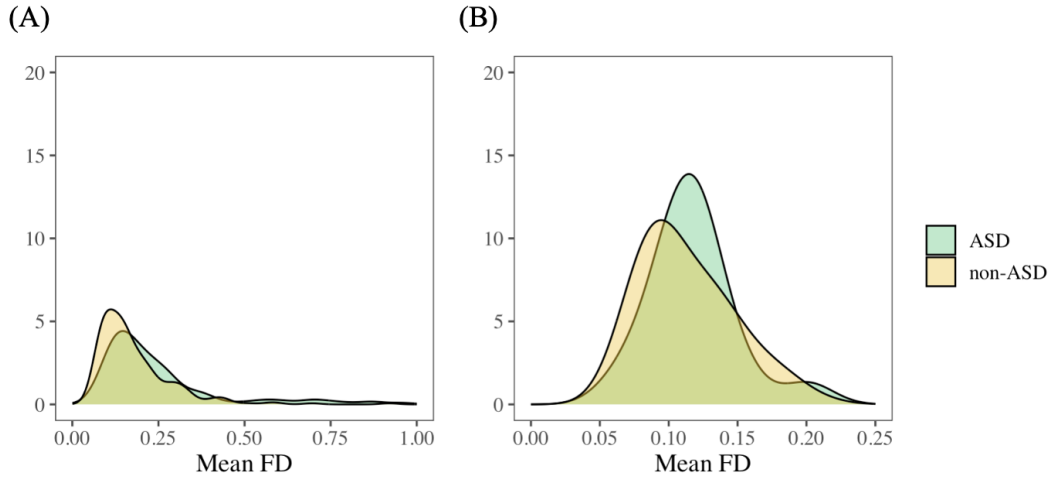


Fig. 1: Distributions of mean framewise displacement (FD) in the school-age children dataset. Panel A shows the distribution of mean FD over all children. Panel B shows the distribution of mean FD over children who meet the inclusion criteria. The distribution of motion in non-ASD children that pass motion quality control differs from the distribution of motion in children with ASD that pass motion quality control.

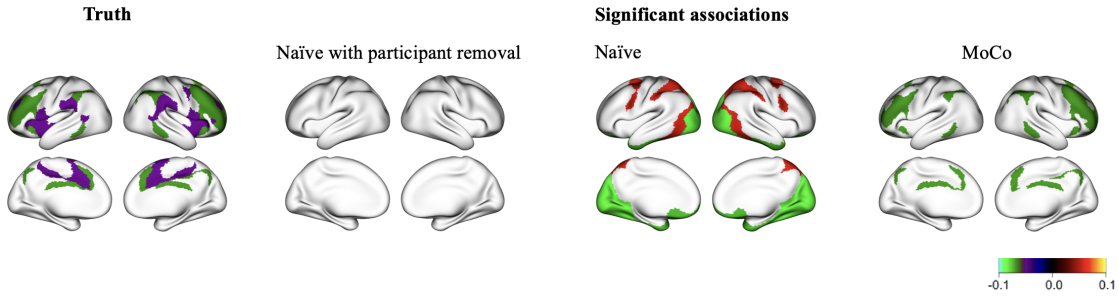


Fig. 2: Example from one simulated dataset. The true association is marked in dark green and purple, while other regions have zero associations. MoCo identified one of the two true associations correctly. However, the naïve method with participant removal missed both regions; the naïve method with all data caused false positives and failed to detect any of the true associations.

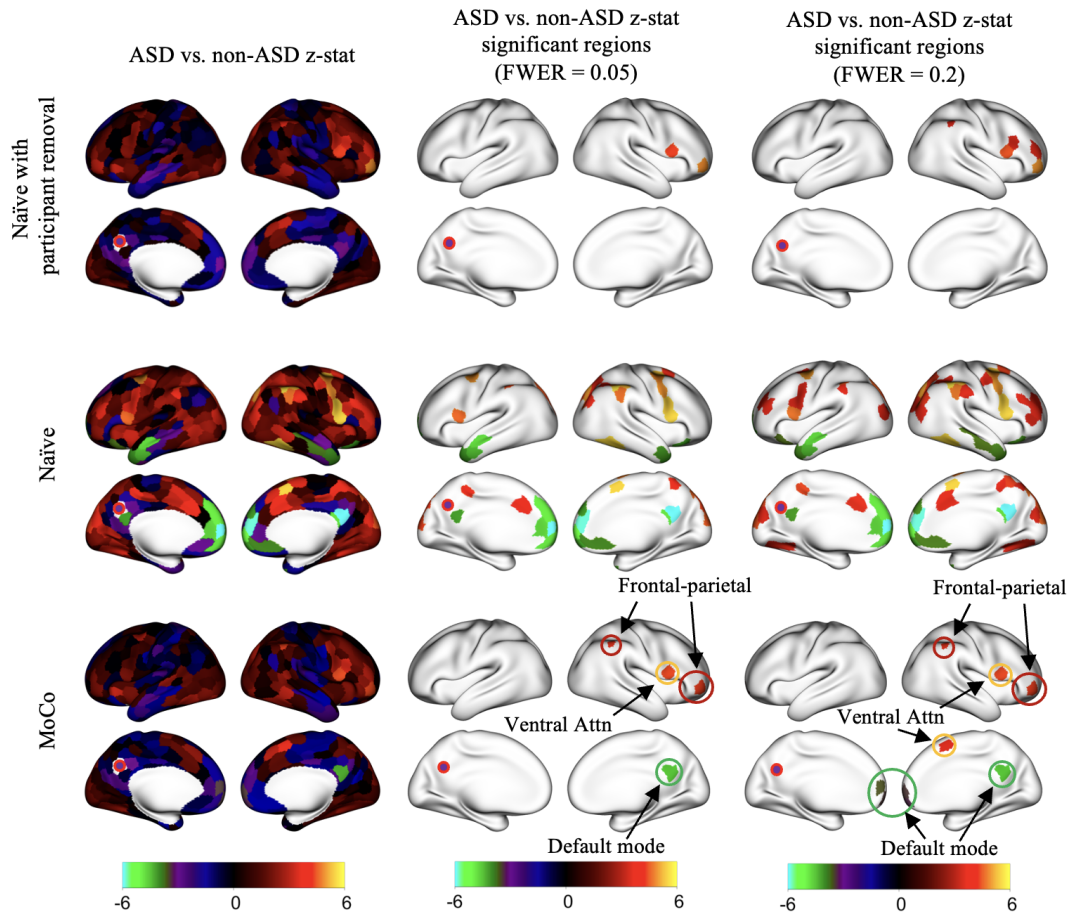


Fig. 3: Z-statistics for the group difference (ASD – non-ASD) for a seed in the posterior default mode network (fuchsia point) in the ABIDE dataset. Extensive hypoconnectivity between the seed region and anterior parts of the default mode network in the naïve approach are likely due to motion artifacts. MoCo appears to effectively control motion artifacts, as the likely spurious differences are removed, and the results look more similar to the naïve approach with participant removal. At FWER=0.05, MoCo also identifies frontal-parietal hyperconnectivity not detected in the naïve approaches.

True association		MoCo	naïve with participant removal	naïve	
Region 1	0	Bias	0.0005	-0.0190	-0.0644
		sd	0.0372	0.0191	0.0204
		MSE $\times 10^3$	1.3839	0.7283	4.5657
		Type I error	0.0110	0.1070	0.8670
Region 2	0	Bias	0.0048	0.0176	0.0611
		sd	0.0238	0.0234	0.0221
		MSE $\times 10^3$	0.5894	0.8576	4.2200
		Type I error	0.0100	0.0730	0.7220
Region 3	0	Bias	0.0044	0.0153	0.0553
		sd	0.0183	0.0179	0.0182
		MSE $\times 10^3$	0.3554	0.5542	3.3941
		Type I error	0.0080	0.0680	0.8320
Region 4	0	Bias	-0.0034	-0.0179	-0.0663
		sd	0.0204	0.0199	0.0204
		MSE $\times 10^3$	0.4275	0.7180	4.8182
		Type I error	0.0100	0.1160	0.8870
Region 5	-0.0484	Bias	0.0065	0.0213	0.0695
		sd	0.0214	0.0208	0.0212
		MSE $\times 10^3$	0.4990	0.8848	5.2748
		Power	0.3790	0.1700	0.1260
Region 6	-0.0682	Bias	0.0063	0.0241	0.0796
		sd	0.0203	0.0178	0.0214
		MSE $\times 10^3$	0.4523	0.8979	6.7937
		Power	0.8690	0.5280	0.0670

Table 2: Simulation results comparing MoCo, the naïve approach with participant removal, and the naïve approach including all participants. MoCo has lower bias in all regions, lower type I error in regions in which the true association is zero, and higher power in the regions where true association is non-zero.

Nonparametric motion control in functional connectivity studies in children with autism spectrum disorder

SUPPLEMENTARY MATERIAL

1 Identifying motion-controlled association of ASD and brain connectivity

Theorem 1.1 *Under (A1)-(A3), the counterfactual $\theta_{C,a}$ is identified by θ_a , where $\theta_a = \iiint \mu_{Y|A,Z,M,X}(a, z, m, x) p_{Z|A,X}(z | a, x) p_{M|\Delta=1,A,X}(m | 0, x) p_X(x) dz dm dx$.*

Proof Let $\theta_{C,a} = E\{E_C[Y(M_0) | A = a, X]\}$, where $M_0 \sim P_{M|\Delta=1,A,X}(m | 0, x)$. We have:

$$\begin{aligned}
\theta_{C,a} &= E\{E_C[Y(M_0) | A = a, X]\} \\
&= \int E_C(Y(M_0) | A = a, X = x) p_X(x) dx \\
&\stackrel{\text{tower rule}}{=} \iint E_C(Y(m) | M_0 = m, A = a, X = x) p_{M|\Delta=1,A,X}(m | 0, x) p_X(x) dm dx \\
&\stackrel{\text{defn}}{=} \iint E_C(Y(m) | A = a, X = x) p_{M|\Delta=1,A,X}(m | 0, x) p_X(x) dm dx \\
&\stackrel{\text{tower rule}}{=} \iiint E_C(Y(m) | A = a, X = x, Z = z) p_{Z|A,X}(z | a, x) p_{M|\Delta=1,A,X}(m | 0, x) p_X(x) dz dm dx \\
&\stackrel{\text{assumption (A2)}}{=} \iiint E_C(Y(m) | M = m, A = a, X = x, Z = z) p_{Z|A,X}(z | a, x) p_{M|\Delta=1,A,X}(m | 0, x) p_X(x) dz dm dx \\
&\stackrel{\text{assumption (A3)}}{=} \iiint E(Y | M = m, A = a, X = x, Z = z) p_{Z|A,X}(z | a, x) p_{M|\Delta=1,A,X}(m | 0, x) p_X(x) dz dm dx .
\end{aligned}$$

The fourth equality results from the fact that by the construction of M_0 , we have that $Y(m) \perp\!\!\!\perp M_0 | A, X$ for all m . The sixth equality results from the assumption that $Y(m) \perp\!\!\!\perp M | A, X, Z$.

2 Efficient influence function Theorem 3.1

2.1 Overview of efficiency theory

The efficient influence function can be used to characterize the nonparametric efficiency bound, i.e., the smallest asymptotic variance of any regular, *asymptotically linear* estimator of θ_a (Bickel and others, 1993). An estimator $\theta_{n,a}$ of θ_a based on $O_1, \dots, O_n \stackrel{\text{i.i.d}}{\sim} P$ is said to be asymptotically linear if there exists a function $o \mapsto \tilde{D}_{P,a}(o)$ such that $E[\tilde{D}_{P,a}(O)] = 0$, $E[\tilde{D}_{P,a}^2(O)] < \infty$, and

$\theta_{n,a} = \theta_a + n^{-1} \sum_{i=1}^n \tilde{D}_{P,a}(O_i) + o_P(n^{-1/2})$. We refer to $\tilde{D}_{P,a}$ as the *influence function* of $\theta_{n,a}$. Under this representation, the asymptotic study of $\theta_{n,a}$ reduces to the study of the sample mean $n^{-1} \sum_{i=1}^n \tilde{D}_{P,a}(O_i)$ whose large sample behavior can be described using standard results such as the weak law of large numbers and the central limit theorem. The latter implies $n^{1/2}(\theta_{n,a} - \theta_a)$ converges to a mean-zero normal random variable with variance equal to $E[\tilde{D}_{P,a}^2(O)]$. Due to the fact that the asymptotic variance of an asymptotically linear estimator is characterized by the variance of the influence function, the influence function that has the smallest variance amongst all influence functions of regular estimators is called the *efficient influence function*. An estimator with an influence function equal to the efficient influence function is, by definition, asymptotically efficient.

2.2 Proof of Theorem 3.1

Proof Let \mathcal{P} be the model for the true distribution. Let $o = (a, m, \delta, x, z, y)$ denote values of the observed vector of variable $O = (A, M, \Delta, X, Z, Y)$, and $O \sim P \in \mathcal{P}$. We use $\Psi_a : \mathcal{P} \rightarrow \mathbb{R}$ to denote a parameter as a functional that maps the distribution P in the model \mathcal{P} to the real number θ_a .

$$\begin{aligned} \Psi_a(P) &= \iiint \mu_{Y|A,M,X,Z}(a, m, x, z) p_{Z|A,X}(z | a, x) p_{M|\Delta=1,A,X}(m | 0, x) p_X(x) dz dmdx \\ &= \int y dP_{Y|A,M,X,Z}(y | a, m, x, z) dP_{Z|A,X}(z | a, x) dP_{M|\Delta=1,A,X}(m | 0, x) dP_X(x) . \end{aligned}$$

We consider a collection of submodels through P at $\epsilon = 0$ in the direction S , $\{P_\epsilon \in \mathcal{P}, dP_\epsilon = (1 + \epsilon S)dP\}$ where S is an element of the Hilbert space $L_0^2(P)$, the space of all functions of O such that $\int S(o)dP(o) = 0$, $\int S(o)^2 dP(o) < \infty$ equipped with inner product $\langle f, g \rangle = \int f(o)g(o)dP(o)$. We consider the derivative of the parameter mapping along the path P_ϵ . We can view this derivative as a bounded functional on $L_0^2(P)$, which, by the Reisz representation theorem, will have an inner-product form $\langle s, D_P \rangle$ for a unique element $D_P \in L_0^2(P)$. D_P is referred to as the *canonical gradient* of Ψ_a . This gradient will also be the efficient influence function of regular asymptotically linear estimators of Ψ_a . Thus, to derive the efficient influence function, we may study the following derivative of Ψ_a and write that derivative in an inner product form (Levy, 2019). Below, we use the notation $\int f(o)dP_0(o)$ interchangeably with $\int f(o)P_0(do)$ to denote the Lebesgue integral of a P_0 -measurable function f with respect to probability measure P_0 .

$$\begin{aligned} \left. \frac{\partial}{\partial \epsilon} \Psi_a(P_\epsilon) \right|_{\epsilon=0} &= \left. \frac{\partial}{\partial \epsilon} \int y dP_{\epsilon,Y|A,M,X,Z}(y | a, m, x, z) dP_{\epsilon,Z|A,X}(z | a, x) dP_{\epsilon,M|\Delta=1,A,X}(m | 0, x) dP_{\epsilon,X}(x) \right|_{\epsilon=0} \\ &= \int y S_{Y|A,M,X,Z}(y | a, m, x, z) dP_{Y|A,M,X,Z}(y | a, m, x, z) dP_{Z|A,X}(z | a, x) dP_{M|\Delta=1,A,X}(m | 0, x) dP_X(x) \end{aligned} \quad (2.1)$$

$$+ \int y S_{Z|A,X}(z | a, x) dP_{Y|A,M,X,Z}(y | a, m, x, z) dP_{Z|A,X}(z | a, x) dP_{M|\Delta=1,A,X}(m | 0, x) dP_X(x) \quad (2.2)$$

$$+ \int y S_{M|\Delta=1,A,X}(m | 0, x) dP_{Y|A,M,X,Z}(y | a, m, x, z) dP_{Z|A,X}(z | a, x) dP_{M|\Delta=1,A,X}(m | 0, x) dP_X(x) \quad (2.3)$$

$$+ \int y S_X(x) dP_{Y|A,M,X,Z}(y | a, m, x, z) dP_{Z|A,X}(z | a, x) dP_{M|\Delta=1,A,X}(m | 0, x) dP_X(x) \quad (2.4)$$

where

$$\begin{aligned}
dP_{\epsilon, Y|A, M, X, Z}(y | a, m, x, z) &= \frac{\int_{\delta} (1 + \epsilon S(o)) P(a, m, d\delta, x, z, y)}{\int_{\delta, y} (1 + \epsilon S(o)) P(a, m, d\delta, x, z, dy)}, \\
S_{Y|A, M, X, Z}(y | a, m, x, z) &= \left. \frac{\partial \log dP_{\epsilon, Y|A, M, X, Z}(y | a, m, x, z)}{\partial \epsilon} \right|_{\epsilon=0} = E(S(O) | y, a, m, x, z) - E(S(O) | a, m, x, z), \\
dP_{\epsilon, Z|A, X}(y | a, x) &= \frac{\int_{\delta, m, y} (1 + \epsilon S(o)) P(a, dm, d\delta, x, z, dy)}{\int_{\delta, m, y, z} (1 + \epsilon S(o)) P(a, dm, d\delta, x, dz, dy)}, \\
S_{Z|A, X}(z | a, x) &= \left. \frac{\partial \log dP_{\epsilon, Z|A, X}(y | a, x)}{\partial \epsilon} \right|_{\epsilon=0} = E(S(O) | z, a, x) - E(S(O) | a, x), \\
dP_{\epsilon, M|\Delta=1, A, X}(m | 0, x) &= \frac{\int_{z, y} \mathbb{1}_{0,1}(a, \delta) (1 + \epsilon S(o)) P(a, m, \delta, x, dz, dy)}{\int_{m, z, y} \mathbb{1}_{0,1}(a, \delta) (1 + \epsilon S(o)) P(a, dm, \delta, x, dz, dy)}, \\
S_{M|\Delta=1, A, X}(m | 0, x) &= \left. \frac{\partial \log P_{\epsilon, M|\Delta=1, A, X}(m | 0, x)}{\partial \epsilon} \right|_{\epsilon=0} = E(S(O) \mathbb{1}_{0,1}(A, \Delta) | m, a, \delta, x) - E(S(O) \mathbb{1}_{0,1}(A, \Delta) | a, \delta, x), \\
dP_{\epsilon, X}(x) &= \int_{\delta, a, m, y, z} (1 + \epsilon S(o)) P(da, dm, d\delta, x, dz, dy), \\
S_X(x) &= E(S(O) | x) .
\end{aligned}$$

Evaluating the derivative for the term (2.1), we have:

$$\begin{aligned}
(2.1) \int y S_{Y|A, M, X, Z}(y | a, m, x, z) P_{Y|A, M, X, Z}(y | a, m, x, z) dP_{Z|A, X}(z | a, x) dP_{M|\Delta=1, A, X}(m | 0, x) dP_X(x) \\
&= \int \frac{\mathbb{1}_a(a')}{\pi_{a'}(x)} y S_{Y|A, M, X, Z}(y | a', m, x, z) dP_{Y|A, M, X, Z}(y | a', m, x, z) dP_{Z|A, X}(z | a', x) dP_{M|\Delta=1, A, X}(m | 0, x) dP_{A, X}(a', x) \\
&= \int \frac{\mathbb{1}_a(a')}{\pi_{a'}(x)} \frac{p_{M|\Delta=1, A, X}(m | 0, x)}{p_{M|A, X, Z}(m | a', x, z)} y S_{Y|A, M, X, Z}(y | a', m, x, z) dP_{Y|A, M, X, Z}(y | a', m, x, z) \\
&\quad dP_{M|A, X, Z}(m | a', x, z) dP_{Z|A, X}(z | a', x) dP_{A, X}(a', x) \\
&= \int \frac{\mathbb{1}_a(a')}{\pi_{a'}(x)} \frac{p_{M|\Delta=1, A, X}(m | 0, x)}{p_{M|A, X, Z}(m | a', x, z)} y S_{Y|A, M, X, Z}(y | a', m, x, z) dP(o) \\
&\stackrel{*}{=} \int \frac{\mathbb{1}_a(a')}{\pi_{a'}(x)} \frac{p_{M|\Delta=1, A, X}(m | 0, x)}{p_{M|A, X, Z}(m | a', x, z)} (y - \mu_{Y|A, M, X, Z}(a, m, x, z)) S_{Y|A, M, X, Z}(y | a', m, x, z) dP(o) \\
&\stackrel{**}{=} \int \frac{\mathbb{1}_a(a')}{\pi_a(x)} \frac{p_{M|\Delta=1, A, X}(m | 0, x)}{p_{M|A, X, Z}(m | a, x, z)} (y - \mu_{Y|A, M, X, Z}(a, m, x, z)) S(o) dP(o) .
\end{aligned}$$

The reason for (*) is:

$$\int \frac{\mathbb{1}_a(a')}{\pi_{a'}(x)} \frac{p_{M|\Delta=1, A, X}(m | 0, x)}{p_{M|A, X, Z}(m | a', x, z)} \mu_{Y|A, M, X, Z}(a, m, x, z) S_{Y|A, M, X, Z}(y | a', m, x, z) dP(o) = 0 .$$

The reason for (**) is:

$$\begin{aligned}
S_{Y, A, M, X, Z}(y, a', m, x, z) &= S_{Y|A, M, X, Z}(y | a', m, x, z) + S_{A, M, X, Z}(a', m, x, z) , \\
\int \frac{\mathbb{1}_a(a')}{\pi_a(x)} \frac{p_{M|\Delta=1, A, X}(m | 0, x)}{p_{M|A, X, Z}(m | a, x, z)} (y - \mu_{Y|A, M, X, Z}(a, m, x, z)) S_{A, M, X, Z}(a', m, x, z) dP(o) &= 0 , \\
S(o) &= S_{Y, A, M, X, Z}(y, a', m, x, z) + S_{\Delta|Y, A, M, X, Z}(\delta | y, a', m, x, z) .
\end{aligned}$$

The same logic can be applied to evaluate term (2.2)-(2.4). We have,

$$\begin{aligned}
(2.2) \quad & \int y S_{Z|A,X}(z | a, x) dP_{Y|A,M,X,Z}(y | a, m, x, z) dP_{Z|A,X}(z | a, x) dP_{M|\Delta=1,A,X}(m | 0, x) dP_X(x) \\
&= \int \eta_{\mu|A,X,Z}(a, x, z) S_{Z|A,X}(z | a, x) dP_{Z|A,X}(z | a, x) dP_X(x) \\
&= \int \frac{\mathbb{1}_a(a')}{\pi_{a'}(x)} \eta_{\mu|A,X,Z}(a', x, z) S_{Z|A,X}(z | a', x) dP_{Z|A,X}(z | a', x) dP(a', x) \\
&= \int \frac{\mathbb{1}_a(a')}{\pi_{a'}(x)} (\eta_{\mu|A,X,Z}(a', x, z) - \xi_{a,\eta|X}(x)) S_{Z|A,X}(z | a', x) dP(o) \\
&= \int \frac{\mathbb{1}_a(a')}{\pi_a(x)} (\eta_{\mu|A,X,Z}(a, x, z) - \xi_{a,\eta|X}(x)) S(o) dP(o) .
\end{aligned}$$

$$\begin{aligned}
(2.3) \quad & \int y S_{M|\Delta=1,A,X}(m | 0, x) dP_{Y|A,M,X,Z}(y | a, m, x, z) dP_{Z|A,X}(z | a, x) dP_{M|\Delta=1,A,X}(m | 0, x) dP_X(x) \\
&= \int \eta_{\mu|A,M,X}(a, m, x) S_{M|\Delta=1,A,X}(m | 0, x) dP_{M|\Delta=1,A,X}(m | 0, x) dP_X(x) \\
&= \int \frac{\mathbb{1}_{0,1}(a', \Delta)}{\bar{\pi}_0(x)} \eta_{\mu|A,M,X}(a, m, x) S_{M|\Delta=1,A,X}(m | 0, x) dP_{M,\Delta=1,A,X}(m, \delta = 1, a' = 0, x) \\
&= \int \frac{\mathbb{1}_{0,1}(a', \Delta)}{\bar{\pi}_0(x)} (\eta_{\mu|A,M,X}(a, m, x) - \xi_{a,\eta|X}(x)) S_{M|\Delta=1,A,X}(m | 0, x) dP(o) \\
&= \int \frac{\mathbb{1}_{0,1}(a', \Delta)}{\bar{\pi}_0(x)} (\eta_{\mu|A,M,X}(a, m, x) - \xi_{a,\eta|X}(x)) S(o) dP(o) .
\end{aligned}$$

$$\begin{aligned}
(2.4) \quad & \int y S_X(x) dP_{Y|A,M,X,Z}(y | a, m, x, z) dP_{Z|A,X}(z | a, x) dP_{M|\Delta=1,A,X}(m | 0, x) dP_X(x) \\
&= \int \xi_{a,\eta|X}(x) S_X(x) dP_X(x) \\
&= \int (\xi_{a,\eta|X}(x) - \theta_a) S(o) dP(o) .
\end{aligned}$$

Putting the results together, we have:

$$\begin{aligned}
\left. \frac{\partial}{\partial \epsilon} \Psi_a(P_\epsilon) \right|_{\epsilon=0} &= \int \frac{\mathbb{1}_a(a')}{\pi_a(x)} \frac{p_{M|\Delta=1,A,X}(m | 0, x)}{p_{M|A,X,Z}(m | a, x, z)} (y - \mu_{Y|A,M,X,Z}(a, m, x, z)) S(o) dP(o) \\
&\quad + \int \frac{\mathbb{1}_a(a')}{\pi_a(x)} (\eta_{\mu|A,X,Z}(a, x, z) - \xi_{a,\eta|X}(x)) S(o) dP(o) \\
&\quad + \int \frac{\mathbb{1}_{0,1}(a', \Delta)}{\bar{\pi}_0(x)} (\eta_{\mu|A,M,X}(a, m, x) - \xi_{a,\eta|X}(x)) S(o) dP(o) \\
&\quad + \int (\xi_{a,\eta|X}(x) - \theta_a) S(o) dP(o) .
\end{aligned}$$

Thus, we have expressed the derivative of Ψ_a along a path P_ϵ as an inner product between S and the gradient:

$$\begin{aligned}
D_{P,a}(O_i) &= \frac{\mathbb{1}_a(A_i)}{\pi_a(X_i)} \frac{p_{M|\Delta=1,A,X}(M_i | 0, X_i)}{p_{M|A,X,Z}(M_i | A_i, X_i, Z_i)} \{Y_i - \mu_{Y|A,M,X,Z}(a, M_i, X_i, Z_i)\} \\
&\quad + \frac{\mathbb{1}_a(A_i)}{\pi_a(X_i)} \{ \eta_{\mu|A,Z,X}(a, X_i, Z_i) - \xi_{a,\eta|X}(X_i) \} \\
&\quad + \frac{\mathbb{1}_{0,1}(A_i, \Delta_i)}{\bar{\pi}_0(X_i)} \{ \eta_{\mu|A,M,X}(a, M_i, X_i) - \xi_{a,\eta|X}(X_i) \} \\
&\quad + \xi_{a,\eta|X}(X_i) - \theta_a .
\end{aligned}$$

As the tangent space of our model is $L_0^2(P_0)$, there is only a single gradient for Ψ_a . Thus, this gradient is by definition the efficient gradient and the efficient influence function for regular asymptotically Normal estimators of $\Psi_a(P_0)$.

3 Consistency of the one-step estimator

3.1 Proof of Theorem 3.2

3.1.1 Part I

For fixed a , we define $D_{P,a}^* = D_{P,a} + \theta_a$. $D_{P,a}^*$ corresponds to the first three lines and the first term of the fourth line in equation (3.5) of the main manuscript. We rewrite $D_{P,a}^*$ as

$$\begin{aligned} D_{P,a}^*(O) &= \frac{\mathbb{1}_a(A)}{\pi_a(X)} \frac{p_{M|\Delta=1,A,X}(M|0,X)}{p_{M|A,X,Z}(M|A,X,Z)} \{Y - \mu_{Y|A,M,X,Z}(a, M, X, Z)\} \\ &\quad + \frac{\mathbb{1}_a(A)}{\pi_a(X)} \eta_{\mu|A,Z,X}(a, X, Z) \\ &\quad + \frac{\mathbb{1}_{0,1}(A, \Delta)}{\bar{\pi}_0(X)} \{\eta_{\mu|A,M,X}(a, M, X) - \xi_{a,\eta|X}(X)\} \\ &\quad + \xi_{a,\eta|X}(X) - \frac{\mathbb{1}_a(A)}{\pi_a(X)} \xi_{a,\eta|X}(X). \end{aligned}$$

Consider a probability distribution $P' \in \mathcal{P}$. Next we show that, if any one of the conditions in assumption (ii) holds, then $E[D_{P',a}^*(O)] - \theta_a = 0$.

$$\begin{aligned} E[D_{P',a}^*(O)] - \theta_a &= E \left[\frac{\mathbb{1}_a(A)}{\pi'_a(X)} \frac{p'_{M|\Delta=1,A,X}(M|0,X)}{p'_{M|A,X,Z}(M|A,X,Z)} \{Y - \mu'_{Y|A,M,X,Z}(a, M, X, Z)\} \right] \\ &\quad + E \left[\frac{\mathbb{1}_a(A)}{\pi'_a(X)} \eta'_{\mu|A,Z,X}(a, X, Z) \right] \\ &\quad + E \left[\frac{\mathbb{1}_{0,1}(A, \Delta)}{\bar{\pi}'_0(X)} \{\eta'_{\mu|A,M,X}(a, M, X) - \xi'_{a,\eta|X}(X)\} \right] \\ &\quad + E \left[\xi'_{a,\eta|X}(X) - \frac{\mathbb{1}_a(A)}{\pi'_a(X)} \xi'_{a,\eta|X}(X) \right] \\ &\quad - \theta_a. \end{aligned}$$

We derive the precise expression for each term:

$$\begin{aligned} &E \left[\frac{\mathbb{1}_a(A)}{\pi'_a(X)} \frac{p'_{M|\Delta=1,A,X}(M|0,X)}{p'_{M|A,X,Z}(M|A,X,Z)} \{Y - \mu'_{Y|A,M,X,Z}(a, M, X, Z)\} \right] \\ &= \int \frac{\mathbb{1}_a(a^*)}{\pi'_a(X)} \frac{p'_{M|\Delta=1,A,X}(m|0,x)}{p'_{M|A,X,Z}(m|a^*,x,z)} \{y - \mu'_{Y|A,M,X,Z}(a, m, x, z)\} p_{A,M,X,Z,Y}(a^*, m, x, z, y) da^* dm dz dx dy \\ &= \int \frac{\mathbb{1}_a(a^*)}{\pi'_a(X)} \frac{p'_{M|\Delta=1,A,X}(m|0,x)}{p'_{M|A,X,Z}(m|a,x,z)} \left\{ \int y p_{Y|A,M,X,Z}(y|a,m,x,z) dy - \mu'_{Y|A,M,X,Z}(a, m, x, z) \right\} \\ &\quad p_{A,M,X,Z}(a, m, x, z) da^* dm dz dx \\ &= \int \frac{\mathbb{1}_a(a^*) \pi_a(x) da^*}{\pi'_a(X)} \frac{p'_{M|\Delta=1,A,X}(m|0,x)}{p'_{M|A,X,Z}(m|a,x,z)} \{ \mu_{Y|A,M,X,Z}(a, m, x, z) - \mu'_{Y|A,M,X,Z}(a, m, x, z) \} \\ &\quad p_{M|A,X,Z}(m|a,x,z) p_{Z|A,X}(z|a,x) p_X(x) dm dz dx \\ &= \int \frac{\pi_a(x)}{\pi'_a(x)} \frac{p'_{M|\Delta=1,A,X}(m|0,x)}{p'_{M|A,X,Z}(m|a,x,z)} \{ \mu_{Y|A,M,X,Z}(a, m, x, z) - \mu'_{Y|A,M,X,Z}(a, m, x, z) \} \\ &\quad p_{M|A,X,Z}(m|a,x,z) p_{Z|A,X}(z|a,x) p_X(x) dm dz dx. \end{aligned} \tag{3.1}$$

$$\begin{aligned}
& E \left[\frac{\mathbb{1}_a(A)}{\pi'_a(X)} \eta'_{\mu|A,Z,X}(a, X, Z) \right] \\
&= \int \frac{\mathbb{1}_a(a^*)}{\pi'_a(X)} \eta'_{\mu|A,Z,X}(a, x, z) p_{A,X,Z}(a^*, x, z) da^* dz dx \\
&= \int \frac{\mathbb{1}_a(a^*)}{\pi'_a(X)} \eta'_{\mu|A,Z,X}(a, x, z) p_{Z|A,X}(a, x) \pi_a(x) p_X(x) da^* dz dx \\
&= \int \frac{\int \mathbb{1}_a(a^*) \pi_a(x) da^*}{\pi'_a(X)} \eta'_{\mu|A,Z,X}(a, x, z) p_{Z|A,X}(a, x) p_X(x) dz dx \\
&= \int \frac{\pi_a(x)}{\pi'_a(x)} \eta'_{\mu|A,Z,X}(a, x, z) p_{Z|A,X}(a, x) p_X(x) dz dx .
\end{aligned} \tag{3.2}$$

$$\begin{aligned}
& E \left[\frac{\mathbb{1}_{0,1}(A, \Delta)}{\bar{\pi}'_0(X)} \{ \eta'_{\mu|A,M,X}(a, M, X) - \xi'_{a,\eta|X}(X) \} \right] \\
&= \int \frac{\mathbb{1}_{0,1}(a^*, \Delta)}{\bar{\pi}'_0(X)} \eta'_{\mu|A,M,X}(a, m, x) p_{A,\Delta,M,X}(a^*, \Delta, m, x) da^* d\Delta dmdx \\
&\quad - \int \frac{\mathbb{1}_{0,1}(a^*, \Delta)}{\bar{\pi}'_0(X)} \xi'_{a,\eta|X}(x) p_{A,\Delta,X}(a^*, \Delta, x) da^* d\Delta dx \\
&= \int \frac{\mathbb{1}_{0,1}(a^*, \Delta)}{\bar{\pi}'_0(X)} \eta'_{\mu|A,M,X}(a, m, x) p_{M|\Delta=1,A,X}(m | 0, x) \bar{\pi}_0(x) p_X(x) da^* d\Delta dmdx \\
&\quad - \int \frac{\mathbb{1}_{0,1}(a^*, \Delta)}{\bar{\pi}'_0(X)} \xi'_{a,\eta|X}(x) \bar{\pi}_0(x) p_X(x) da^* d\Delta dx \\
&= \int \frac{\int \mathbb{1}_{0,1}(a^*, \Delta) \bar{\pi}_0(x) da^* d\Delta}{\bar{\pi}'_0(X)} \eta'_{\mu|A,M,X}(a, m, x) p_{M|\Delta=1,A,X}(m | 0, x) p_X(x) dmdx \\
&\quad - \int \frac{\int \mathbb{1}_{0,1}(a^*, \Delta) \bar{\pi}_0(x) da^* d\Delta}{\bar{\pi}'_0(X)} \xi'_{a,\eta|X}(x) p_X(x) dx \\
&= \int \frac{\bar{\pi}_0(x)}{\bar{\pi}'_0(x)} \eta'_{\mu|A,M,X}(a, m, x) p_{M|\Delta=1,A,X}(m | 0, x) p_X(x) dmdx \\
&\quad - \int \frac{\bar{\pi}_0(x)}{\bar{\pi}'_0(x)} \eta'_{\mu|A,M,X}(a, m, x) p'_{M|\Delta=1,A,X}(m | 0, x) p_X(x) dmdx \\
&= \int \frac{\bar{\pi}_0(x)}{\bar{\pi}'_0(x)} \eta'_{\mu|A,M,X}(a, m, x) \{ p_{M|\Delta=1,A,X}(m | 0, x) - p'_{M|\Delta=1,A,X}(m | 0, x) \} p_X(x) dmdx .
\end{aligned} \tag{3.3}$$

$$\begin{aligned}
& E \left[\xi'_{a,\eta|X}(X) - \frac{\mathbb{1}_a(A)}{\pi'_a(X)} \xi'_{a,\eta|X}(X) \right] \\
&= \int \xi'_{a,\eta|X}(x) p_X(x) dx - \int \frac{\mathbb{1}_a(a^*)}{\pi'_a(X)} \xi'_{a,\eta|X}(x) p_{A,X}(a^*, x) da^* dx \\
&= \int \xi'_{a,\eta|X}(x) p_X(x) dx - \int \frac{\pi_a(x)}{\pi'_a(x)} \xi'_{a,\eta|X}(x) p_X(x) dx \\
&= \int \xi'_{a,\eta|X}(x) \left\{ 1 - \frac{\pi_a(x)}{\pi'_a(x)} \right\} p_X(x) dx .
\end{aligned} \tag{3.4}$$

$$-\theta_a = - \int \xi'_{a,\eta|X}(x) p_X(x) dx . \tag{3.5}$$

Therefore,

$$E[D_{P',a}^*(O)] - \theta_a = (3.1) + (3.2) + (3.3) + (3.4) + (3.5) .$$

First, note that

$$\begin{aligned}
(3.4) + (3.5) &= \int \xi'_{a,\eta|X}(x) \left\{ 1 - \frac{\pi_a(x)}{\pi'_a(x)} \right\} p_X(x) dx - \int \xi_{a,\eta|X}(x) p_X(x) dx \\
&= \int \left\{ \xi'_{a,\eta|X}(x) - \xi_{a,\eta|X}(x) \right\} \left\{ 1 - \frac{\pi_a(x)}{\pi'_a(x)} \right\} p_X(x) dx \\
&\quad - \int \xi_{a,\eta|X}(x) \frac{\pi_a(x)}{\pi'_a(x)} p_X(x) dx .
\end{aligned} \tag{3.6}$$

Using the definition of $\xi_{a,\eta|X}(x)$ in the main manuscript, we obtain

$$\begin{aligned}
&\int \xi_{a,\eta|X}(x) \frac{\pi_a(x)}{\pi'_a(x)} p_X(x) dx = \\
&\int \frac{\pi_a(x)}{\pi'_a(x)} \frac{p_{M|\Delta=1,A,X}(m|0,x)}{p_{M|A,X,Z}(m|a,x,z)} \left\{ \mu_{Y|A,M,X,Z}(a,m,x,z) - \mu'_{Y|A,M,X,Z}(a,m,x,z) \right\} p_{M|A,X,Z}(m|a,x,z) p_{Z|A,X}(z|a,x) p_X(x) dmdzdx \\
&+ \int \frac{\pi_a(x)}{\pi'_a(x)} p_{M|\Delta=1,A,X}(m|0,x) \mu'_{Y|A,M,X,Z}(a,m,x,z) p_{Z|A,X}(z|a,x) p_X(x) dmdzdx .
\end{aligned} \tag{3.7}$$

Thus

$$\begin{aligned}
(3.1) + (3.4) + (3.5) &= (3.6) - (3.7) \\
&+ \int \frac{\pi_a(x)}{\pi'_a(x)} \left\{ \frac{p'_{M|\Delta=1,A,X}(m|0,x)}{p'_{M|A,X,Z}(m|a,x,z)} - \frac{p_{M|\Delta=1,A,X}(m|0,x)}{p_{M|A,X,Z}(m|a,x,z)} \right\} \times \\
&\left\{ \mu_{Y|A,M,X,Z}(a,m,x,z) - \mu'_{Y|A,M,X,Z}(a,m,x,z) \right\} p_{M|A,X,Z}(m|a,x,z) p_{Z|A,X}(z|a,x) p_X(x) dmdzdx .
\end{aligned} \tag{3.8}$$

We also have

$$(3.2) - (3.7) = \int \frac{\pi_a(x)}{\pi'_a(x)} \left\{ p'_{M|\Delta=1,A,X}(m|0,x) - p_{M|\Delta=1,A,X}(m|0,x) \right\} \mu'_{Y|A,M,X,Z}(a,m,x,z) p_{Z|A,X}(z|a,x) p_X(x) dmdzdx ,$$

which yields

$$\begin{aligned}
(3.2) + (3.3) - (3.7) &= \int \frac{\bar{\pi}_0(x)}{\bar{\pi}'_0(x)} \eta'_{\mu|A,M,X}(a,m,x) (p_{M|\Delta=1,A,X}(m|0,x) - p'_{M|\Delta=1,A,X}(m|0,x)) p_X(x) dmdx \\
&+ \int \frac{\pi_a(x)}{\pi'_a(x)} \left\{ p'_{M|\Delta=1,A,X}(m|0,x) - p_{M|\Delta=1,A,X}(m|0,x) \right\} \mu_{Y|A,M,X,Z}(a,m,x,z) p_{Z|A,X}(z|a,x) p_X(x) dmdzdx \\
&+ \int \frac{\pi_a(x)}{\pi'_a(x)} \left\{ p'_{M|\Delta=1,A,X}(m|0,x) - p_{M|\Delta=1,A,X}(m|0,x) \right\} \left\{ \mu'_{Y|A,M,X,Z}(a,m,x,z) - \mu_{Y|A,M,X,Z}(a,m,x,z) \right\} \\
&p_{Z|A,X}(z|a,x) p_X(x) dmdzdx \\
&= - \int \frac{\bar{\pi}_0(x)}{\bar{\pi}'_0(x)} \eta'_{\mu|A,M,X}(a,m,x) \left\{ p'_{M|\Delta=1,A,X}(m|0,x) - p_{M|\Delta=1,A,X}(m|0,x) \right\} p_X(x) dmdx \\
&+ \int \frac{\pi_a(x)}{\pi'_a(x)} \eta_{\mu|A,M,X}(a,m,x) \left\{ p'_{M|\Delta=1,A,X}(m|0,x) - p_{M|\Delta=1,A,X}(m|0,x) \right\} p_X(x) dmdx \\
&+ \int \frac{\pi_a(x)}{\pi'_a(x)} \left\{ p'_{M|\Delta=1,A,X}(m|0,x) - p_{M|\Delta=1,A,X}(m|0,x) \right\} \left\{ \mu'_{Y|A,M,X,Z}(a,m,x,z) - \mu_{Y|A,M,X,Z}(a,m,x,z) \right\} \\
&p_{Z|A,X}(z|a,x) p_X(x) dmdzdx \\
&= \int \left\{ \frac{\pi_a(x)}{\pi'_a(x)} \eta_{\mu|A,M,X}(a,m,x) - \frac{\bar{\pi}_0(x)}{\bar{\pi}'_0(x)} \eta'_{\mu|A,M,X}(a,m,x) \right\} \left\{ p'_{M|\Delta=1,A,X}(m|0,x) - p_{M|\Delta=1,A,X}(m|0,x) \right\} p_X(x) dmdx \\
&\tag{3.9} \\
&+ \int \frac{\pi_a(x)}{\pi'_a(x)} \left\{ p'_{M|\Delta=1,A,X}(m|0,x) - p_{M|\Delta=1,A,X}(m|0,x) \right\} \left\{ \mu'_{Y|A,M,X,Z}(a,m,x,z) - \mu_{Y|A,M,X,Z}(a,m,x,z) \right\} \\
&p_{Z|A,X}(z|a,x) p_X(x) dmdzdx .
\end{aligned} \tag{3.10}$$

Putting everything together yields

$$(3.1) + (3.2) + (3.3) + (3.4) + (3.5) = (3.6) + (3.8) + (3.9) + (3.10) .$$

Thus,

$$\begin{aligned} & E [D_{P',a}^*(O)] - \theta_a \\ = & \int \{ \xi'_{a,\eta|X}(x) - \xi_{a,\eta|X}(x) \} \left(1 - \frac{\pi_a(x)}{\pi'_a(x)} \right) p_X(x) dx \\ & + \int \frac{\pi_a(x)}{\pi'_a(x)} \left\{ \frac{p'_{M|\Delta=1,A,X}(m|0,x)}{p'_{M|A,X,Z}(m|a,x,z)} - \frac{p_{M|\Delta=1,A,X}(m|0,x)}{p_{M|A,X,Z}(m|a,x,z)} \right\} \times \\ & \{ \mu_{Y|A,M,X,Z}(a,m,x,z) - \mu'_{Y|A,M,X,Z}(a,m,x,z) \} p_{M|A,X,Z}(m|a,x,z) p_{Z|A,X}(z|a,x) p_X(x) dmdzdx \\ & + \int \left\{ \frac{\pi_a(x)}{\pi'_a(x)} \eta_{\mu|A,M,X}(a,m,x) - \frac{\bar{\pi}_0(x)}{\bar{\pi}'_0(x)} \eta'_{\mu|A,M,X}(a,m,x) \right\} \{ p'_{M|\Delta=1,A,X}(m|0,x) - p_{M|\Delta=1,A,X}(m|0,x) \} p_X(x) dmdx \\ & + \int \frac{\pi_a(x)}{\pi'_a(x)} \{ p'_{M|\Delta=1,A,X}(m|0,x) - p_{M|\Delta=1,A,X}(m|0,x) \} \{ \mu'_{Y|A,M,X,Z}(a,m,x,z) - \mu_{Y|A,M,X,Z}(a,m,x,z) \} \\ & p_{Z|A,X}(z|a,x) p_X(x) dmdzdx . \end{aligned}$$

3.1.2 Part II

Let P_n denote the empirical measure of O_1, \dots, O_n . Let P'_n be any estimator of P_0 compatible with the nuisance models used in the estimation of $D_{P,a}$, we have:

$$\begin{aligned} \Psi_a(P'_n) - \Psi_a(P) &= (P'_n - P) D_{P'_n,a} + R_2(P, P'_n) \\ &= -P D_{P'_n,a} + R_2(P, P'_n) \\ &= -P_n D_{P'_n,a} + (P_n - P) D_{P,a} + (P_n - P)(D_{P'_n,a} - D_{P,a}) + R_2(P, P'_n) , \end{aligned}$$

where $R_2(P, P'_n)$ is the second-order remainder term. As the one-step estimator is defined as $\Psi_a(P'_n) + P_n D_{P'_n,a}$, we have:

$$\theta_{n,a}^+ - \theta_a = (P_n - P) D_{P,a} + (P_n - P)(D_{P'_n,a} - D_{P,a}) + R_2(P, P'_n) .$$

Next, we need to show $(P_n - P)(D_{P'_n,a} - D_{P,a}) = o_P(1)$ and $R_2(P, P'_n) = o_P(1)$. The former will hold under conditions (B3) and (B4) of the theorem.

As for the second order reminder term, we have:

$$R_2(P, P'_n) = \Psi_a(P'_n) + P D_{P'_n,a} - \Psi_a(P) = E [D_{P'_n,a}^*(O)] - \theta_a .$$

Referring back to Part I, we have

$$\begin{aligned} & R_2(P, P'_n) \\ = & \int \{ \xi_{n,a,\eta|X}(x) - \xi_{a,\eta|X}(x) \} \left(1 - \frac{\pi_a(x)}{\pi_{n,a}(x)} \right) p_X(x) dx \\ & + \int \frac{\pi_a(x)}{\pi_{n,a}(x)} \left\{ \frac{p_{n,M|\Delta=1,A,X}(m|0,x)}{p_{n,M|A,X,Z}(m|a,x,z)} - \frac{p_{M|\Delta=1,A,X}(m|0,x)}{p_{M|A,X,Z}(m|a,x,z)} \right\} \times \\ & \{ \mu_{Y|A,M,X,Z}(a,m,x,z) - \mu_{n,Y|A,M,X,Z}(a,m,x,z) \} p_{M|A,X,Z}(m|a,x,z) p_{Z|A,X}(z|a,x) p_X(x) dmdzdx \\ & + \int \left\{ \frac{\pi_a(x)}{\pi_{n,a}(x)} \eta_{\mu|A,M,X}(a,m,x) - \frac{\bar{\pi}_0(x)}{\bar{\pi}_{n,0}(x)} \eta_{n,\mu|A,M,X}(a,m,x) \right\} \{ p_{n,M|\Delta=1,A,X}(m|0,x) - p_{M|\Delta=1,A,X}(m|0,x) \} p_X(x) dmdx \\ & + \int \frac{\pi_a(x)}{\pi_{n,a}(x)} \{ p_{n,M|\Delta=1,A,X}(m|0,x) - p_{M|\Delta=1,A,X}(m|0,x) \} \{ \mu_{n,Y|A,M,X,Z}(a,m,x,z) - \mu_{Y|A,M,X,Z}(a,m,x,z) \} \\ & p_{Z|A,X}(z|a,x) p_X(x) dmdzdx . \end{aligned}$$

Using Cauchy-Schwartz inequality and assumptions (B1) and (B2) of the theorem, we can show $R_2(P, P'_n) = o_P(1)$. To be more specific, for the first line of the term,

$$\begin{aligned} & \int \{ \xi_{n,a,\eta|X}(x) - \xi_{a,\eta|X}(x) \} \left(1 - \frac{\pi_a(x)}{\pi_{n,a}(x)} \right) p_X(x) dx \\ & \leq \int \left| \{ \xi_{n,a,\eta|X}(x) - \xi_{a,\eta|X}(x) \} \left(\frac{\pi_{n,a}(x) - \pi_a(x)}{\pi_{n,a}(x)} \right) p_X(x) \right| dx \\ & \leq \left\{ \sup_x \frac{1}{\pi_{n,a}(x)} \right\} \int \left| \{ \xi_{n,a,\eta|X}(x) - \xi_{a,\eta|X}(x) \} \{ \pi_{n,a}(x) - \pi_a(x) \} \right| p_X(x) dx . \end{aligned}$$

Then applying assumption (B1) to the supremum and Cauchy-Schwarz to the integration, we have

$$\begin{aligned} & \leq \frac{1}{\epsilon_1} \| \xi_{n,\eta|a,X} - \xi_{a,\eta|X} \| \| \pi_{n,a} - \pi_a \| \\ & = o_P(1) , \end{aligned}$$

where the last line follows from assumption (B2). The same reasoning can be extended to the other terms in $R_2(P, P'_n)$.

For the second line of the term,

$$\begin{aligned} & \int \frac{\pi_a(x)}{\pi_{n,a}(x)} \left\{ \frac{p_{n,M|\Delta=1,A,X}(m | 0, x)}{p_{n,M|A,X,Z}(m | a, x, z)} - \frac{p_{M|\Delta=1,A,X}(m | 0, x)}{p_{M|A,X,Z}(m | a, x, z)} \right\} \times \\ & \left\{ \mu_{Y|A,M,X,Z}(a, m, x, z) - \mu_{n,Y|A,M,X,Z}(a, m, x, z) \right\} p_{M|A,X,Z}(m | a, x, z) p_{Z|A,X}(z | a, x) p_X(x) dm dz dx \\ & = \int \frac{\pi_a(x)}{\pi_{n,a}(x)} \left\{ \frac{p_{n,M|\Delta=1,A,X}(m | 0, x) - p_{M|\Delta=1,A,X}(m | 0, x)}{p_{n,M|A,X,Z}(m | a, x, z)} \right\} \times \\ & \left\{ \mu_{Y|A,M,X,Z}(a, m, x, z) - \mu_{n,Y|A,M,X,Z}(a, m, x, z) \right\} p_{M|A,X,Z}(m | a, x, z) p_{Z|A,X}(z | a, x) p_X(x) dm dz dx \\ & + \int \frac{\pi_a(x)}{\pi_{n,a}(x)} \left\{ \frac{p_{M|A,X,Z}(m | a, x, z) - p_{n,M|A,X,Z}(m | a, x, z)}{p_{n,M|A,X,Z}(m | a, x, z)} \right\} \times \\ & \left\{ \mu_{Y|A,M,X,Z}(a, m, x, z) - \mu_{n,Y|A,M,X,Z}(a, m, x, z) \right\} p_{M|\Delta=1,A,X}(m | 0, x) p_{Z|A,X}(z | a, x) p_X(x) dm dz dx \\ & \leq \left\{ \sup_{m,a,x,z} \frac{1}{\pi_{n,a}(x) p_{n,M|A,X,Z}(m | a, x, z)} \right\} \int \left| \left\{ p_{n,M|\Delta=1,A,X}(m | 0, x) - p_{M|\Delta=1,A,X}(m | 0, x) \right\} \times \right. \\ & \quad \left. \left\{ \mu_{Y|A,M,X,Z}(a, m, x, z) - \mu_{n,Y|A,M,X,Z}(a, m, x, z) \right\} \right| p_{M|A,X,Z}(m | a, x, z) p_{Z|A,X}(z | a, x) p_X(x) dx \\ & + \left\{ \sup_{m,a,x,z} \frac{1}{\pi_{n,a}(x) p_{n,M|A,X,Z}(m | a, x, z)} \right\} \int \left| \left\{ p_{M|A,X,Z}(m | a, x, z) - p_{n,M|A,X,Z}(m | a, x, z) \right\} \times \right. \\ & \quad \left. \left\{ \mu_{Y|A,M,X,Z}(a, m, x, z) - \mu_{n,Y|A,M,X,Z}(a, m, x, z) \right\} \right| p_{M|\Delta=1,A,X}(m | 0, x) p_{Z|A,X}(z | a, x) p_X(x) dx \\ & \leq \frac{1}{\epsilon_1 \epsilon_3} \| p_{n,M|\Delta=1,A,X}(m | 0, x) - p_{M|\Delta=1,A,X}(m | 0, x) \| \| \mu_{Y|A,M,X,Z}(a, m, x, z) - \mu_{n,Y|A,M,X,Z}(a, m, x, z) \| \\ & + \frac{1}{\epsilon_1 \epsilon_3} \| p_{M|A,X,Z}(m | a, x, z) - p_{n,M|A,X,Z}(m | a, x, z) \| \| \mu_{Y|A,M,X,Z}(a, m, x, z) - \mu_{n,Y|A,M,X,Z}(a, m, x, z) \| \\ & = o_p(1) . \end{aligned}$$

For the third line of the term,

$$\begin{aligned}
& \int \left\{ \frac{\pi_a(x)}{\pi_{n,a}(x)} \eta_{\mu|A,M,X}(a, m, x) - \frac{\bar{\pi}_0(x)}{\bar{\pi}_{n,0}(x)} \eta_{n,\mu|A,M,X}(a, m, x) \right\} \{p_{n,M|\Delta=1,A,X}(m | 0, x) - p_{M|\Delta=1,A,X}(m | 0, x)\} p_X(x) dmdx \\
&= \int \left\{ \frac{\pi_a(x) - \pi_{n,a}(x)}{\pi_{n,a}(x)} \eta_{\mu|A,M,X}(a, m, x) + \frac{\bar{\pi}_{n,0}(x) - \bar{\pi}_0(x)}{\bar{\pi}_{n,0}(x)} \eta_{\mu|A,M,X}(a, m, x) + \frac{\bar{\pi}_0(x)}{\bar{\pi}_{n,0}(x)} \{ \eta_{\mu|A,M,X}(a, m, x) - \eta_{n,\mu|A,M,X}(a, m, x) \} \right\} \times \\
&\quad \{p_{n,M|\Delta=1,A,X}(m | 0, x) - p_{M|\Delta=1,A,X}(m | 0, x)\} p_X(x) dmdx \\
&\leq \left\{ \sup_x \frac{1}{\pi_{n,a}(x)} \right\} \int |\{\pi_a(x) - \pi_{n,a}(x)\} \{p_{n,M|\Delta=1,A,X}(m | 0, x) - p_{M|\Delta=1,A,X}(m | 0, x)\}| \eta_{\mu|A,M,X}(a, m, x) p_X(x) dmdx \\
&+ \left\{ \sup_x \frac{1}{\bar{\pi}_{n,0}(x)} \right\} \int |\{\bar{\pi}_{n,0}(x) - \bar{\pi}_0(x)\} \{p_{n,M|\Delta=1,A,X}(m | 0, x) - p_{M|\Delta=1,A,X}(m | 0, x)\}| \eta_{\mu|A,M,X}(a, m, x) p_X(x) dmdx \\
&+ \left\{ \sup_x \frac{1}{\bar{\pi}_{n,0}(x)} \right\} \int |\{\eta_{\mu|A,M,X}(a, m, x) - \eta_{n,\mu|A,M,X}(a, m, x)\} \{p_{n,M|\Delta=1,A,X}(m | 0, x) - p_{M|\Delta=1,A,X}(m | 0, x)\}| \bar{\pi}_0(x) p_X(x) dmdx \\
&\leq \frac{1}{\epsilon_1} \|\pi_a(x) - \pi_{n,a}(x)\| \|p_{n,M|\Delta=1,A,X}(m | 0, x) - p_{M|\Delta=1,A,X}(m | 0, x)\| \\
&+ \frac{1}{\epsilon_2} \|\bar{\pi}_{n,0}(x) - \bar{\pi}_0(x)\| \|p_{n,M|\Delta=1,A,X}(m | 0, x) - p_{M|\Delta=1,A,X}(m | 0, x)\| \\
&+ \frac{1}{\epsilon_2} \|\eta_{\mu|A,M,X}(a, m, x) - \eta_{n,\mu|A,M,X}(a, m, x)\| \|p_{n,M|\Delta=1,A,X}(m | 0, x) - p_{M|\Delta=1,A,X}(m | 0, x)\| \\
&= o_p(1).
\end{aligned}$$

For the last line of the term,

$$\begin{aligned}
& \int \frac{\pi_a(x)}{\pi_{n,a}(x)} \{p_{n,M|\Delta=1,A,X}(m | 0, x) - p_{M|\Delta=1,A,X}(m | 0, x)\} \{ \mu_{n,Y|A,M,X,Z}(a, m, x, z) - \mu_{Y|A,M,X,Z}(a, m, x, z) \} \\
&\quad p_{Z|A,X}(z | a, x) p_X(x) dmdzdx \\
&\leq \left\{ \sup_x \frac{1}{\pi_{n,a}(x)} \right\} \int |\{p_{n,M|\Delta=1,A,X}(m | 0, x) - p_{M|\Delta=1,A,X}(m | 0, x)\}| \times \\
&\quad \left| \{ \mu_{n,Y|A,M,X,Z}(a, m, x, z) - \mu_{Y|A,M,X,Z}(a, m, x, z) \} \right| p_{Z|A,X}(z | a, x) \pi_a(x) p_X(x) dmdzdx \\
&\leq \frac{1}{\epsilon_1} \|p_{n,M|\Delta=1,A,X}(m | 0, x) - p_{M|\Delta=1,A,X}(m | 0, x)\| \|\mu_{n,Y|A,M,X,Z}(a, m, x, z) - \mu_{Y|A,M,X,Z}(a, m, x, z)\| \\
&= o_p(1).
\end{aligned}$$

Thus $R_2(P, P'_n) = o_p(1)$, thereby concluding the proof.

4 Theorem 3.3

4.1 Assumptions of theorem

Assumption (B1) guarantees that estimated propensities and motion densities are appropriately bounded so that the one-step estimator is never ill-defined. Assumption (C1) stipulates convergence rate conditions on nuisance estimates in terms of $L^2(P)$ norms. This assumption would be satisfied, for example, if each nuisance estimate achieved a rate of at least $n^{-1/4}$ with respect to $L^2(P)$ norm. However, it is also possible for slower convergence rates attained by some nuisance estimators to be compensated for by faster convergence rates attained by others. We note that the $n^{-1/4}$ rate is slower than the standard parametric rate, which potentially allows for the use of flexible regression techniques. On the other hand, to achieve this rate if X and/or Z are high-dimensional may require additional smoothness assumptions on the underlying nuisance parameters. For example, the highly adaptive LASSO estimator achieves a sufficiently fast rate of convergence *if* the underlying nuisance parameters have a *bounded variation norm* (Benkeser and van der Laan, 2016), an assumption that becomes more restrictive in higher dimensions. Assumptions (B3) and (C2) are necessary to ensure the negligibility of an empirical process term (Van Der Vaart and others, 1996). Assumption (C2)

can be eliminated by utilizing cross-fitting techniques (van der Laan *and others*, 2011; Chernozhukov *and others*, 2018).

4.2 Proof of Theorem 3.3

The proof of Theorem 3.3 closely parallels the proof of Theorem 3.2.

$$\theta_{n,a}^+ - \theta_a = (P_n - P)D_{P,a} + (P_n - P)(D_{P'_n,a} - D_{P,a}) + R_2(P, P'_n) .$$

For asymptotic linearity, we need to show $(P_n - P)(D_{P'_n,a} - D_{P,a}) = o_P(1/\sqrt{n})$ and $R_2(P, P'_n) = o_P(1/\sqrt{n})$. The former holds under conditions (B3) and (C2) of the theorem. The structure of the second-order term is presented in the proof of Theorem 3.2, Part I, and the convergence of the second-order term is established using logic similar to the proof of Theorem 3.2, Part II.

5 Simulation details

Sex X_1 was generated from a Bernoulli distribution with a probability of 0.75 of female sex, age X_2 was generated by truncating a Gamma distribution with a shape of 25 and a rate of 2.5 to values between 8 and 13, and right-handedness X_3 was simulated from a Bernoulli distribution with success probability of 0.92. Given covariates $X = x$, diagnosis A was drawn from a Bernoulli distribution with a success probability of $\text{expit}(-0.11 + 0.71x_1 - 0.08x_2 - 0.19x_3)$, where these coefficients were derived from a logistic regression fitted to the real data. Diagnosis-specific covariates Z included four components: ADOS Z_1 was assigned a value of 0 for simulated non-ASD participants, while for simulated ASD participants, a value was drawn from a Poisson distribution with mean 11.86; FIQ Z_2 was sampled from a Normal(114.6, 11.6²) distribution for simulated non-ASD participants and a Normal(104.2, 17.4²) distribution for simulated ASD participants, where these means and standard deviations were calculated based on the real data; stimulant and non-stimulant medication, Z_3 and Z_4 , respectively, were assigned a value of 0 for simulated non-ASD participants and had a value drawn from a Bernoulli distribution with success probabilities of 0.2 and 0.17, respectively for $A = 1$ participants. Given $A = a, X = x, Z = z$, the natural logarithm of mean framewise displacement M was generated from a Normal($-1.26 + 0.095a + 0.104x_1 - 0.0535x_2 - 0.12x_3 + 0.00675z_1 - 0.000255z_2 + 0.324z_3 + 0.064z_4, 0.56^2$) distribution. We defined a tolerable motion level $\Delta = 1$ as the indicator that $M \leq 0.2$.

The conditional means of the six functional connectivity outcomes were

$$\mu_{Y_1|A,M,X,Z}(a, m, x, z) = -0.22 + 0 \times a - 0.98m - 0.06x_1 + 0.012x_2 + 0.03x_3,$$

$$\mu_{Y_2|A,M,X,Z}(a, m, x, z) = -0.20 + 0 \times a + 0.92m + 0.06x_1 - 0.009x_2 - 0.03x_3,$$

$$\mu_{Y_3|A,M,X,Z}(a, m, x, z) = -0.37 + 0 \times a + 0.86m + 0.04x_1 + 0.002x_2 + 0.04x_3,$$

$$\mu_{Y_4|A,M,X,Z}(a, m, x, z) = 0.17 + 0 \times a - 1.02m - 0.06x_1 + 0.002x_3 + 0.04x_3,$$

$$\mu_{Y_5|A,M,X,Z}(a, m, x, z)$$

$$= -0.20 - 0.03a + 1.50m - 0.61m^2 + 0.02(x_1 - z_4) - 0.002x_2 + 0.03(x_3 - z_3) - 0.0005z_1 + 0.0003z_2,$$

$$\mu_{Y_6|A,M,X,Z}(a, m, x, z)$$

$$= -0.16 - 0.05a + 1.67m - 0.64m^2 + 0.03(x_1 - z_4) - 0.001x_2 + 0.02(x_3 - z_3) - 0.0005z_1 + 0.0003z_2.$$

6 Additional simulations to confirm theoretical properties of estimators

We evaluate the statistical properties of our estimators established by our theorems through Monte Carlo simulation. These simulations were conducted purely to confirm theoretical properties of the estimators and are not tied to the real data analysis context in any way. In this simulation, we generated covariate X from Bernoulli(1/2). Given $X = x$, we generated a binary variable A according to a Bernoulli distribution with $\pi_1(x) = \text{expit}(x - 1/4)$. Given $A = a$, we drew Z from Bernoulli($\text{expit}(5a/4 - 1/2)$). Given $A = a, X = x, Z = z$, we drew M from a normal distribution $N(1 + a + x/2 - z/4, 1)$. Finally, given $A = a, X = x, Z = z, M = m$, we drew Y is drawn from a normal distribution $N(-1 + x/2 - z/3 - a/4 + m/5, 1)$. We defined a tolerable M level $\Delta = 1$ as the indicator that $M \leq 2$. The true values of these parameters were -0.717 and -1.068, respectively, with variance bound $\text{Var}\{D_{a,P}(O)\}$ equal to 3.453 and 7.151, respectively.

For each sample size $n \in \{200, 500, 1000, 2000, 4000\}$, we generated 1000 datasets based on the above data generating process, and used the resultant data to compute our proposed estimators along with their corresponding confidence interval, either with cross-fitting or without the use of cross-fitting. We evaluated the estimators based on their bias (scaled by $n^{1/2}$), their standard error (scaled by $n^{1/2}$), the ratio of the scaled standard error to the square root of the efficient variance, and the coverage of 95% Wald-style confidence interval.

We first evaluated estimators under the conditions of the theorem where all nuisance parameters are consistently estimated at appropriate rates. To achieve this, we used the logistic regression model for $\pi_a(x)$ and main term linear model $\mu_{Y|A,M,X,Z}(a, m, x, z)$ and fully saturated (all possible interactions) regression models for the remaining nuisance parameters. In this scenario, the one-step estimators are expected to be consistent and asymptotically linear.

When all the nuisance parameters are estimated consistently at appropriate rates, the bias of the estimators decreases to 0 as the sample size increases, and the coverage of the 95% confidence interval increases to 0.95 (Table 1). Even at a sample size of 200, the bias remains approximately 2% of the true value, and the worst-case coverage of 95% confidence intervals is 86%. Similar results are achieved without the use of cross-fitting (Table 2).

We also studied the impact of inconsistent estimation of different combinations of nuisance parameters. We examined five situations in which only specific combinations of the nuisance parameters were correctly specified, as defined in column 1 of Table 3. Based on its multiple robustness properties, our one-step estimators are expected to maintain consistency across these five scenarios. Nuisance regressions that were incorrectly specified were modeled using only the intercept. Conditional densities that were incorrectly specified were modeled using a Gaussian distribution in which the mean was equal to the sample mean and the standard deviation equal to the sample standard deviation.

Our results indicate that as sample size increases, the bias and standard error decrease across all settings considered, which supports the multiple robustness theory (Table 3 and Table 4).

n	$\theta_{n,0}^{cf}$				$\theta_{n,1}^{cf}$			
	$n^{1/2}$ bias	$n^{1/2}$ sd	sd ratio	cover	$n^{1/2}$ bias	$n^{1/2}$ sd	sd ratio	cover
200	-0.208	2.148	1.122	0.910	-0.143	2.391	1.382	0.860
500	-0.169	1.926	0.996	0.942	-0.165	2.319	1.172	0.912
1000	-0.149	1.918	0.987	0.945	-0.119	2.325	1.100	0.929
2000	-0.058	1.980	1.035	0.941	-0.072	2.421	1.093	0.928
4000	0.011	1.887	1.000	0.946	0.050	2.185	0.961	0.960

Table 1: Confirming theoretical properties of estimators: All nuisance parameters are consistently estimated at appropriate rates with the use of MoCo (with cross-fitting).

n	$\theta_{n,0}^+$				$\theta_{n,1}^+$			
	$n^{1/2}$ bias	$n^{1/2}$ sd	sd ratio	cover	$n^{1/2}$ bias	$n^{1/2}$ sd	sd ratio	cover
200	-0.136	2.035	1.053	0.946	-0.168	2.427	1.249	0.882
500	-0.149	2.007	1.035	0.929	-0.238	2.338	1.122	0.920
1000	-0.102	1.940	1.011	0.943	-0.169	2.331	1.080	0.935
2000	-0.052	1.995	1.049	0.933	-0.144	2.403	1.071	0.934
4000	0.037	1.867	0.989	0.956	0.066	2.251	0.982	0.951

Table 2: Confirming theoretical properties of estimators: All nuisance parameters are consistently estimated at appropriate rates without the use of cross-fitting.

7 Additional details of data analysis

Resting-state fMRI scans were acquired using one of three protocols: 1) a 3T Philips Achieva scanner, 8-channel head coil, repetition time (TR)/echo time (TE)=2500/30 ms, flip angle 75°, 3×3×3 mm voxels, SENSE phase reduction=3, 2 dummy scans, scan duration varied from 5m10s (one subject) to 6m45s (one subject) with most scans at either 5m20s (n=46) or 6m30s (n=99) (KKI); 2) the same but with a 32-channel head coil with most scans 6m30s (n=61) (KKI); 3) a 3T Siemens Allegra scanner, 8-channel head coil, TR/TE=2000/15 ms, flip angle=90°, 3x3x4 mm voxels, scan duration=6:00 (NYU), and we removed the first two volumes. All children also had an anatomical T1 scan collected.

T1 anatomical and rs-fMRI data were processed with the cifti option for cortical surface registration using fMRIPrep, including anatomical tissue segmentation, surface construction, and surface registration, followed by fMRI motion correction, slice-time correction, boundary-based coregistration, and resampling to the fsaverage template (Esteban *and others*, 2019). The detailed output from fMRIPrep is included in Section 7.1. We visually inspected the accuracy of the cortical segmentation using the fMRIPrep quality control html files. We excluded 19 participants due to issues with the cortical segmentation. Issues with fMRIPrep included image homogeneity issues, outliers in brain morphology, and motion during the T1 scan. An example participant that failed this step is included in Figure 1.

Our final study sample was 377 children, with 245 non-autistic children and 132 ASD children. Table 5 displays characteristics of the analysis cohort by ASD diagnosis status.

Setting	n	bias $_{\theta_{n,0}^{cf}}$	sd $_{\theta_{n,0}^{cf}}$	bias $_{\theta_{n,1}^{cf}}$	sd $_{\theta_{n,1}^{cf}}$
(B2.1)	200	0.0500	0.1289	0.0681	0.1455
	500	0.0341	0.1016	0.0558	0.0923
	1000	0.0103	0.0710	0.0470	0.0710
	2000	-0.0007	0.0475	0.0380	0.0504
	4000	-0.0026	0.0170	0.0331	0.0368
(B2.2)	200	-0.0575	0.1164	-0.0510	0.1621
	500	-0.0130	0.0865	-0.0206	0.1125
	1000	-0.0087	0.0594	-0.0252	0.0800
	2000	-0.0044	0.0405	-0.0223	0.0555
	4000	-0.0008	0.0264	-0.0147	0.0400
(B2.3)	200	-0.0412	0.1199	-0.0561	0.1275
	500	-0.0021	0.0892	-0.0073	0.1006
	1000	-0.0019	0.0612	-0.0043	0.0743
	2000	-0.0011	0.0429	-0.0027	0.0520
	4000	0.0008	0.0272	0.0019	0.0375
(B2.4)	200	-0.0585	0.1189	-0.0488	0.1487
	500	-0.0099	0.0915	-0.0087	0.1035
	1000	-0.0092	0.0608	-0.0170	0.0756
	2000	-0.0039	0.0429	-0.0161	0.0532
	4000	-0.0004	0.0272	-0.0105	0.0383
(B2.5)	200	-0.0599	0.1217	-0.0505	0.1556
	500	-0.0118	0.0885	-0.0143	0.1107
	1000	-0.0107	0.0582	-0.0248	0.0794
	2000	-0.0054	0.0397	-0.0230	0.0565
	4000	-0.0008	0.0264	-0.0148	0.0399

Table 3: Bias and standard deviation(sd) of MoCo (with cross-fitting). The settings column indicates which nuisance parameters are consistently estimated based on assumption (B2) in Theorem 3.2 as outlined in the main manuscript.

Setting	n	bias $_{\theta_{n,0}^+}$	sd $_{\theta_{n,0}^+}$	bias $_{\theta_{n,1}^+}$	sd $_{\theta_{n,1}^+}$
(B2.1)	200	0.0195	0.1164	0.0382	0.1646
	500	0.0106	0.1045	0.0371	0.1020
	1000	0.0002	0.0695	0.0363	0.0735
	2000	-0.0059	0.0478	0.0330	0.0518
	4000	-0.0058	0.0188	0.0308	0.0367
(B2.2)	200	-0.0277	0.1275	-0.0064	0.1982
	500	-0.0125	0.0872	-0.0296	0.1214
	1000	-0.0066	0.0596	-0.0212	0.0851
	2000	-0.0048	0.0409	-0.0194	0.0603
	4000	0.0016	0.0255	-0.0138	0.0413
(B2.3)	200	-0.0234	0.1248	-0.0094	0.1707
	500	-0.0058	0.0883	-0.0112	0.1041
	1000	-0.0035	0.0608	-0.0013	0.0770
	2000	-0.0025	0.0425	-0.0003	0.0552
	4000	0.0021	0.0259	0.0034	0.0389
(B2.4)	200	-0.0275	0.1289	-0.0014	0.1824
	500	-0.0101	0.0895	-0.0221	0.1119
	1000	-0.0062	0.0614	-0.0142	0.0803
	2000	-0.0042	0.0428	-0.0135	0.0574
	4000	0.0018	0.0260	-0.0096	0.0399
(B2.5)	200	-0.0277	0.1275	-0.0064	0.1982
	500	-0.0125	0.0872	-0.0296	0.1214
	1000	-0.0066	0.0596	-0.0212	0.0851
	2000	-0.0048	0.0409	-0.0194	0.0603
	4000	0.0016	0.0255	-0.0138	0.0413

Table 4: Bias and standard deviation(sd) of the one-step estimator without the use of cross-fitting. The settings column indicates which nuisance parameters are consistently estimated based on assumption (B2) in Theorem 3.2 as outlined in the main manuscript.

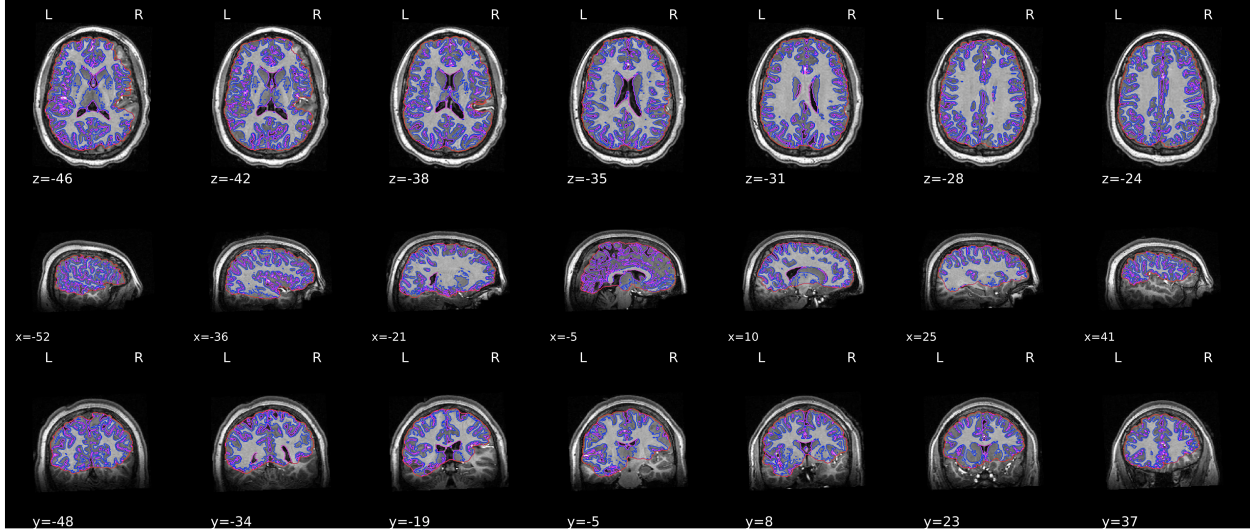


Figure 1: An example participant whose cortical segmentation failed in *fMRIPrep*. The template T1-weighted image is shown with contours outlining the detected brain mask and brain tissue segmentations. It is apparent from the middle and lower rows that large parts of the brain, including most of the temporal lobe and parts of the occipital lobe, were incorrectly excluded from the segmentation.

7.1 *fMRIPrep* data preprocessing for ABIDE

Results included in this manuscript come from preprocessing performed using *fMRIPrep* 21.0.2 (Esteban and others (2018b); Esteban and others (2018a); RRID:SCR_016216), which is based on *Nipype* 1.6.1 (Gorgolewski and others (2011); Gorgolewski and others (2018); RRID:SCR_002502). The text below is automatically produced by *fMRIPrep*.

Anatomical data preprocessing A total of 1 T1-weighted (T1w) images were found within the input BIDS dataset. The T1-weighted (T1w) image was corrected for intensity non-uniformity (INU) with *N4BiasFieldCorrection* (Tustison and others, 2010), distributed with ANTs 2.3.3 (Avants and others, 2008, RRID:SCR_004757), and used as T1w-reference throughout the workflow. The T1w-reference was then skull-stripped with a *Nipype* implementation of the *antsBrainExtraction.sh* workflow (from ANTs), using OASIS30ANTs as target template. Brain tissue segmentation of cerebrospinal fluid (CSF), white-matter (WM) and gray-matter (GM) was performed on the brain-extracted T1w using *fast* (FSL 6.0.5.1:57b01774, RRID:SCR_002823, Zhang and others, 2001). Brain surfaces were reconstructed using *recon-all* (FreeSurfer 6.0.1, RRID:SCR_001847, Dale and others, 1999), and the brain mask estimated previously was refined with a custom variation of the method to reconcile ANTs-derived and FreeSurfer-derived segmentations of the cortical gray-matter of Mindboggle (RRID:SCR_002438, Klein and others, 2017). Volume-based spatial normalization to two standard spaces (MNI152 NLin6 Asym, MNI152 NLin 2009c Asym) was performed through nonlinear registration with *antsRegistration* (ANTs 2.3.3), using brain-extracted versions of both T1w reference and the T1w template. The following templates were selected for spatial normalization: *ICBM 152 Nonlinear Asymmetrical template version 2009c* [Fonov and others (2009), RRID:SCR_008796; TemplateFlow ID: MNI152NLin2009cAsym], *FSL's MNI ICBM 152 non-linear 6th Generation Asymmetric Average Brain Stereotaxic Registra-*

	ASD (N=132)	non-ASD (N=245)	Total (N=377)	p value
Δ				< 0.001
Unusable	98 (74.2%)	119 (48.6%)	217 (57.6%)	
Usable	34 (25.8%)	126 (51.4%)	160 (42.4%)	
Age				0.395
Mean (SD)	10.281 (1.590)	10.413 (1.356)	10.367 (1.441)	
Range	8.014 - 13.950	8.010 - 13.720	8.010 - 13.950	
Gender				0.009
Female	24 (18.2%)	75 (30.6%)	99 (26.3%)	
Male	108 (81.8%)	170 (69.4%)	278 (73.7%)	
Handedness				0.454
Left	12 (9.1%)	17 (6.9%)	29 (7.7%)	
Right	120 (90.9%)	228 (93.1%)	348 (92.3%)	
ADOS				< 0.001
Mean (SD)	11.856 (3.831)	0.000 (0.000)	4.151 (6.098)	
Range	4.000 - 22.000	0.000 - 0.000	0.000 - 22.000	
FIQ				< 0.001
Mean (SD)	104.182 (17.368)	114.649 (11.569)	110.984 (14.729)	
Range	67.000 - 148.000	80.000 - 144.000	67.000 - 148.000	
Currently on Stimulants				< 0.001
No	105 (79.5%)	245 (100.0%)	350 (92.8%)	
Yes	27 (20.5%)	0 (0.0%)	27 (7.2%)	
Currently on Nonstimulants				< 0.001
No	109 (82.6%)	244 (99.6%)	353 (93.6%)	
Yes	23 (17.4%)	1 (0.4%)	24 (6.4%)	
Site ID				< 0.001
ABIDEI-KKI	19 (14.4%)	32 (13.1%)	51 (13.5%)	
ABIDEI-NYU	39 (29.5%)	41 (16.7%)	80 (21.2%)	
ABIDEII-KKI	51 (38.6%)	152 (62.0%)	203 (53.8%)	
ABIDEII-NYU	23 (17.4%)	20 (8.2%)	43 (11.4%)	

Table 5: Demographic characteristics: Continuous variables are described using mean and standard deviation, and diagnostic groups are compared using the Kruskal-Wallis rank-sum test. Binary and categorical variables are reported as frequencies and percentages, and differences between diagnostic groups are assessed using either the Chi-square test or Fisher’s exact test.

tion Model [Evans and others (2012), RRID:SCR_002823; TemplateFlow ID: MNI152NLin6Asym].

Functional data preprocessing For each of the 1 BOLD runs found per subject (across all tasks and sessions), the following preprocessing was performed. First, a reference volume and its skull-stripped version were generated using a custom methodology of *fMRIPrep*. Head-motion parameters with respect to the BOLD reference (transformation matrices, and six corresponding rotation and translation parameters) are estimated before any spatiotemporal filtering using *mcflirt* (FSL 6.0.5.1:57b01774, Jenkinson and others, 2002). BOLD runs were slice-time corrected to 1.22s (0.5 of slice acquisition range 0s-2.45s) using *3dTshift* from AFNI (Cox and Hyde, 1997, RRID:SCR_005927). The BOLD time-series (including slice-timing correction when applied) were resampled onto their original, native space by applying the transforms to correct for head-motion. These resampled BOLD time-series will be referred to as *preprocessed BOLD in original space*, or just *preprocessed BOLD*. The BOLD reference was then co-registered to the T1w reference using *bbregister* (FreeSurfer) which

implements boundary-based registration (Greve and Fischl, 2009). Co-registration was configured with six degrees of freedom. Several confounding time-series were calculated based on the *preprocessed BOLD*: framewise displacement (FD) and three region-wise global signals. FD was computed following Power (absolute sum of relative motions, Power and others (2014)) calculated using the implementation in *Nipype* (following the definitions by Power and others, 2014). The three global signals were extracted within the CSF, the WM, and the whole-brain masks. The BOLD time-series were resampled into standard space, generating a *preprocessed BOLD run in MNI152NLin2009cAsym space*. First, a reference volume and its skull-stripped version were generated using a custom methodology of *fMRIPrep*. The BOLD time-series were resampled onto the following surfaces (FreeSurfer reconstruction nomenclature): *fsaverage*. *Grayordinates* files (Glasser and others, 2013) containing 91k samples were also generated using the highest-resolution *fsaverage* as intermediate standardized surface space. All resamplings can be performed with *a single interpolation step* by composing all the pertinent transformations (i.e. head-motion transform matrices and co-registrations to anatomical and output spaces). Gridded (volumetric) resamplings were performed using *antsApplyTransforms* (ANTs), configured with Lanczos interpolation to minimize the smoothing effects of other kernels (Lanczos, 1964). Non-gridded (surface) resamplings were performed using *mri_vol2surf* (FreeSurfer).

Many internal operations of *fMRIPrep* use *Nilearn* 0.8.1 (Abraham and others, 2014, RRID:SCR_001362), mostly within the functional processing workflow. For more details of the pipeline, see the section corresponding to workflows in *fMRIPrep*'s documentation.

7.1.1 Copyright Waiver

The above boilerplate text was automatically generated by *fMRIPrep* with the express intention that users should copy and paste this text into their manuscripts *unchanged*. It is released under the CC0 license.

7.2 Positivity assumptions in the ABIDE data

For the dataset, the positivity assumption (A1.1) holds as no demographic characteristics X can perfectly predict ASD. To assess the positivity assumptions (A1.2), we examine the values of four ratios present in the estimation process and the efficient influence function:

$$\frac{p_{n,M|\Delta=1,A,X}(M_i | 0, X_i)}{p_{n,M|\Delta=1,A,X,Z}(M_i | A_i, X_i, Z_i)} \text{ for } \Delta_i = 1 \quad (1)$$

$$\frac{p_{n,M|A,X}(M_i | A_i, X_i)}{p_{n,M|A,X,Z}(M_i | A_i, X_i, Z_i)} \quad (2)$$

$$\frac{p_{n,M|\Delta=1,A,X}(M_i | 0, X_i)}{p_{n,M|A,X,Z}(M_i | 0, X_i, Z_i)} \quad (3)$$

$$\frac{p_{n,M|\Delta=1,A,X}(M_i | 0, X_i)}{p_{n,M|A,X,Z}(M_i | 1, X_i, Z_i)}. \quad (4)$$

There are no very large values for these ratios, which indicates the satisfaction of the positivity assumption. Figure 2 displays the histogram depicting the distribution of ratio values.

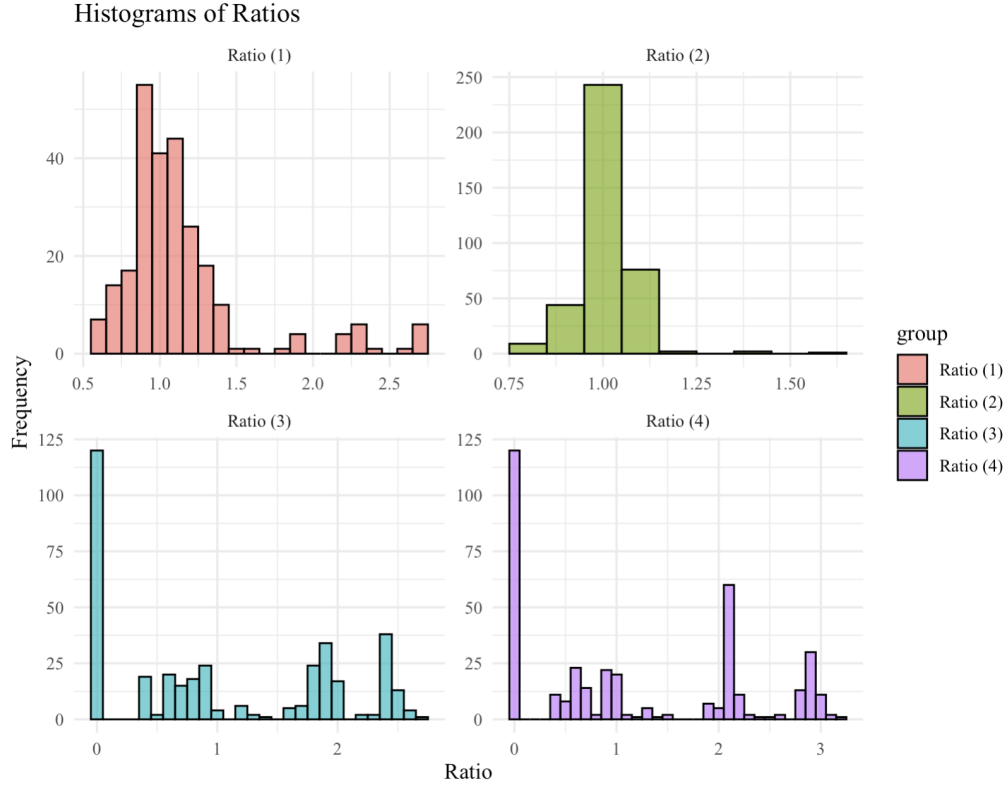


Figure 2: Histogram depicting the distribution of ratio values. Positivity assumptions appear reasonable since the ratios are not too large. Here, the ratios result in reasonable weights in the pseudo-regressions.

7.3 Estimated functional connectivity

The estimated functional connectivity using the naïve approach excluding high-motion participants, the naïve approach including all participants, and MoCo are illustrated in Figure 3. The seed region in the posterior default mode network is defined by the fourteenth parcel but is represented by the fuchsia point for clarity.

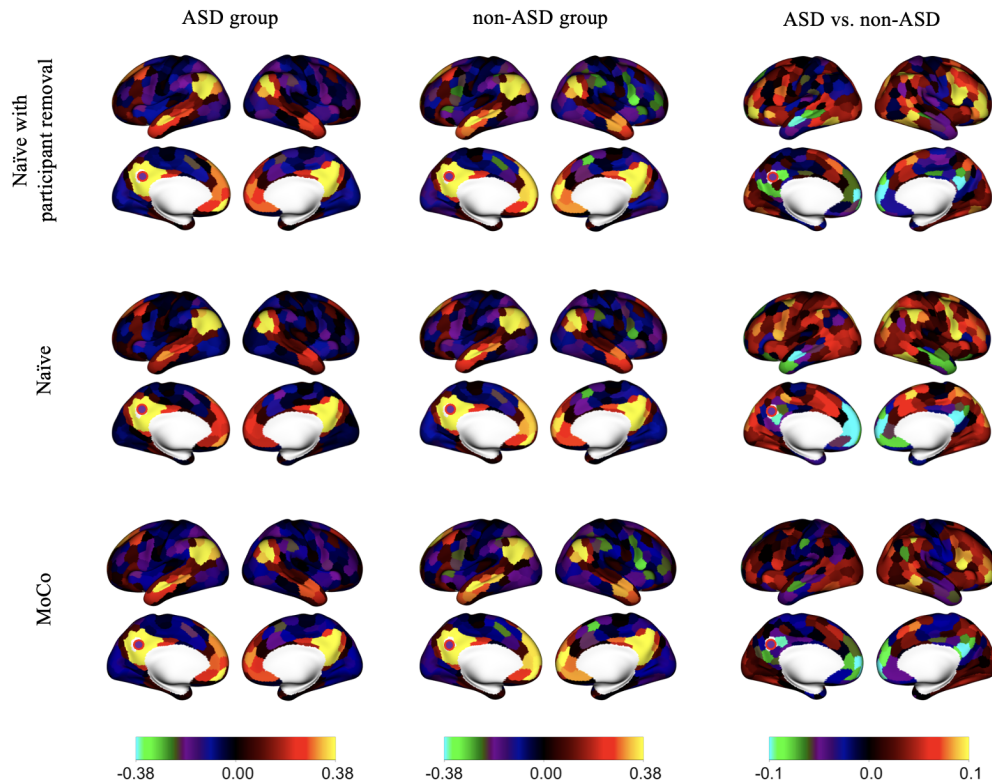


Figure 3: Estimated functional connectivity using the naïve approach excluding high-motion participants, the naïve approach, and MoCo for a seed region in the posterior default mode network (fuchsia point).

References

- ABRAHAM, ALEXANDRE, PEDREGOSA, FABIAN, EICKENBERG, MICHAEL, GERVAIS, PHILIPPE, MUELLER, ANDREAS, KOSSAIFI, JEAN, GRAMFORT, ALEXANDRE, THIRION, BERTRAND AND VAROQUAUX, GAEL. (2014). Machine learning for neuroimaging with scikit-learn. *Frontiers in Neuroinformatics* **8**.
- AVANTS, B.B., EPSTEIN, C.L., GROSSMAN, M. AND GEE, J.C. (2008). Symmetric diffeomorphic image registration with cross-correlation: Evaluating automated labeling of elderly and neurodegenerative brain. *Medical Image Analysis* **12**(1), 26–41.
- BENKESER, DAVID AND VAN DER LAAN, MARK. (2016). The highly adaptive lasso estimator. In: *2016 IEEE International Conference on Data Science and Advanced Analytics (DSAA)*. IEEE. pp. 689–696.
- BICKEL, PETER J, KLAASSEN, CHRIS AJ, RITOV, YA'ACOV AND WELLNER, JON A. (1993). *Efficient and adaptive estimation for semiparametric models*, Volume 4. Springer.
- CHERNOZHUKOV, VICTOR, CHETVERIKOV, DENIS, DEMIRER, MERT, DUFLO, ESTHER, HANSEN, CHRISTIAN, NEWEY, WHITNEY AND ROBINS, JAMES. (2018). Double/debiased machine learning for treatment and structural parameters. *The Econometrics Journal* **21**(1), C1–C68.

- COX, ROBERT W. AND HYDE, JAMES S. (1997). Software tools for analysis and visualization of fmri data. *NMR in Biomedicine* **10**(4-5), 171–178.
- DALE, ANDERS M., FISCHL, BRUCE AND SERENO, MARTIN I. (1999). Cortical surface-based analysis: I. segmentation and surface reconstruction. *NeuroImage* **9**(2), 179–194.
- ESTEBAN, OSCAR, BLAIR, ROSS, MARKIEWICZ, CHRISTOPHER J., BERLEANT, SHOSHANA L., MOODIE, CRAIG, MA, FEILONG, ISIK, AYSE ILKAY, ERRAMUZPE, ASIER, KENT, MATHIAS JAMES D. AND GONCALVES, DUPRE, ELIZABETH, SITEK, KEVIN R., GOMEZ, DANIEL E. P., LURIE, DANIEL J., YE, ZHIFANG, POLDRACK, RUSSELL A. *and others.* (2018a). fmriprep. *Software*.
- ESTEBAN, OSCAR, MARKIEWICZ, CHRISTOPHER, BLAIR, ROSS W, MOODIE, CRAIG, ISIK, AYSE ILKAY, ERRAMUZPE ALIAGA, ASIER, KENT, JAMES, GONCALVES, MATHIAS, DUPRE, ELIZABETH, SNYDER, MADELEINE, OYA, HIROYUKI, GHOSH, SATRAJIT, WRIGHT, JESSEY, DURNEZ, JOKE, POLDRACK, RUSSELL *and others.* (2018b). fMRIPrep: a robust preprocessing pipeline for functional MRI. *Nature Methods*.
- ESTEBAN, OSCAR, MARKIEWICZ, CHRISTOPHER J, BLAIR, ROSS W, MOODIE, CRAIG A, ISIK, A *and others.* (2019). fmriprep: a robust preprocessing pipeline for functional mri. *Nature methods* **16**(1), 111–116.
- EVANS, AC, JANKE, AL, COLLINS, DL AND BAILLET, S. (2012). Brain templates and atlases. *NeuroImage* **62**(2), 911–922.
- FONOV, VS, EVANS, AC, MCKINSTRY, RC, ALMLI, CR AND COLLINS, DL. (2009). Unbiased nonlinear average age-appropriate brain templates from birth to adulthood. *NeuroImage* **47**, **Supplement 1**, S102.
- GLASSER, MATTHEW F., SOTIROPOULOS, STAMATIOS N., WILSON, J. ANTHONY, COALSON, TIMOTHY S., FISCHL, BRUCE, ANDERSSON, JESPER L., XU, JUNQIAN, JBABDI, SAAD, WEBSTER, MATTHEW, POLIMENI, JONATHAN R., VAN ESSEN, DAVID C. *and others.* (2013). The minimal preprocessing pipelines for the human connectome project. *NeuroImage* **80**, 105–124.
- GORGOLEWSKI, K., BURNS, C. D., MADISON, C., CLARK, D., HALCHENKO, Y. O., WASKOM, M. L. AND GHOSH, S. (2011). Nipype: a flexible, lightweight and extensible neuroimaging data processing framework in python. *Frontiers in Neuroinformatics* **5**, 13.
- GORGOLEWSKI, KRZYSZTOF J., ESTEBAN, OSCAR, MARKIEWICZ, CHRISTOPHER J., ZIEGLER, ERIK, ELLIS, DAVID GAGE, NOTTER, MICHAEL PHILIPP, JARECKA, DOROTA, JOHNSON, HANS, BURNS, CHRISTOPHER, MANHÃES-SAVIO, ALEXANDRE, HAMALAINEN, CARLO, YVERNULT, BENJAMIN, SALO, TAYLOR, JORDAN, KESSHI, GONCALVES, MATHIAS, WASKOM, MICHAEL, CLARK, DANIEL, WONG, JASON, LONEY, FRED, MODAT, MARC, DEWEY, BLAKE E, MADISON, CINDEE, VISCONTI DI OLEGGIO CASTELLO, MATTEO, CLARK, MICHAEL G., DAYAN, MICHAEL, CLARK, DAV, KESHAVAN, ANISHA, PINSARD, BASILE, GRAMFORT, ALEXANDRE, BERLEANT, SHOSHANA, NIELSON, DYLAN M., BOUGACHA, SALMA, VAROQUAUX, GAEL, CIPOLLINI, BEN, MARKELLO, ROSS, ROKEM, ARIEL, MOLONEY, BENDAN, HALCHENKO, YAROSLAV O., WASSERMANN, DEMIAN, HANKE, MICHAEL, HOREA, CHRISTIAN, KACZMARZYK, JAKUB, DE HOLLANDER, GILLES, DUPRE, ELIZABETH, GILLMAN, ASHLEY, MORDOM, DAVID, BUCHANAN, COLIN, TUNGARAZA, ROSALIA, PAULI, WOLFGANG M., IQBAL, SHARIQ, SIKKA, SHARAD, MANCINI, MATTEO, SCHWARTZ, YANNICK,

- MALONE, IAN B., DUBOIS, MATHIEU, FROHLICH, CAROLINE, WELCH, DAVID, FORBES, JESSICA, KENT, JAMES, WATANABE, AIMI, CUMBA, CHAD, HUNTENBURG, JULIA M., KASTMAN, ERIK, NICHOLS, B. NOLAN, ESHAGHI, ARMAN, GINSBURG, DANIEL, SCHAEFER, ALEXANDER, ACLAND, BENJAMIN, GIAVASIS, STEVEN, KLEESIEK, JENS, ERICKSON, DREW, KÜTTNER, RENÉ, HASELGROVE, CHRISTIAN, CORREA, CARLOS, GHAYOOR, ALI, LIEM, FRANZ, MILLMAN, JARROD, HAEHN, DANIEL, LAI, JEFF, ZHOU, DALE, BLAIR, ROSS, GLATARD, TRISTAN, RENFRO, MANDY, LIU, SIQI, KAHN, ARI E., PÉREZ-GARCÍA, FERNANDO, TRIPLETT, WILLIAM, LAMPE, LEONIE, STADLER, JÖRG, KONG, XIANG-ZHEN, HALQUIST, MICHAEL, CHETVERIKOV, ANDREY, SALVATORE, JOHN, PARK, ANNE, POLDRACK, RUSSELL, CRADDOCK, R. CAMERON, INATI, SOUHEIL, HINDS, OLIVER, COOPER, GAVIN, PERKINS, L. NATHAN, MARINA, ANA, MATTFELD, AARON, NOEL, MAXIME, SNOEK, LUKAS, MATSUBARA, K, CHEUNG, BRIAN, ROTHMEI, SIMON, URCHS, SEBASTIAN, DURNEZ, JOKE, MERTZ, FRED, GEISLER, DANIEL, FLOREN, ANDREW, GERHARD, STEPHAN, SHARP, PAUL, MOLINA-ROMERO, MIGUEL, WEINSTEIN, ALEJANDRO, BRODERICK, WILLIAM, SAASE, VICTOR, ANDBERG, SAMI KRISTIAN, HARMS, ROBBERT, SCHLAMP, KAI, ARIAS, JAIME, PAPPADOPOULOS ORFANOS, DIMITRI, TARBERT, CLAIRE, TAMBINI, ARIELLE, DE LA VEGA, ALEJANDRO, NICKSON, THOMAS, BRETT, MATTHEW, FALKIEWICZ, MARCEL, PODRANSKI, KORNELIUS, LINKERSDÖRFER, JANOSCH, FLANDIN, GUILLAUME, ORT, EDUARD, SHACHNEV, DMITRY, MCNAMEE, DANIEL, DAVISON, ANDREW, VARADA, JAN, SCHWABACHER, ISAAC, PELLMAN, JOHN, PEREZ-GUEVARA, MARTIN, KHANUJA, RANJEET, PANNETIER, NICOLAS, MCDERMOTTROE, CONOR *and others.* (2018). Nipype. *Software*.
- GREVE, DOUGLAS N AND FISCHL, BRUCE. (2009). Accurate and robust brain image alignment using boundary-based registration. *NeuroImage* **48**(1), 63–72.
- JENKINSON, MARK, BANNISTER, PETER, BRADY, MICHAEL AND SMITH, STEPHEN. (2002). Improved optimization for the robust and accurate linear registration and motion correction of brain images. *NeuroImage* **17**(2), 825–841.
- KLEIN, ARNO, GHOSH, SATRAJIT S., BAO, FORREST S., GIARD, JOACHIM, HÄME, YRJÖ, STAVSKY, ELIEZER, LEE, NOAH, ROSSA, BRIAN, REUTER, MARTIN, NETO, ELIAS CHAIBUB *and others.* (2017). Mindboggling morphometry of human brains. *PLOS Computational Biology* **13**(2), e1005350.
- LANCZOS, C. (1964). Evaluation of noisy data. *Journal of the Society for Industrial and Applied Mathematics Series B Numerical Analysis* **1**(1), 76–85.
- LEVY, JONATHAN. (2019). Tutorial: Deriving the efficient influence curve for large models. *arXiv preprint arXiv:1903.01706*.
- POWER, JONATHAN D., MITRA, ANISH, LAUMANN, TIMOTHY O., SNYDER, ABRAHAM Z., SCHLAGGAR, BRADLEY L. AND PETERSEN, STEVEN E. (2014). Methods to detect, characterize, and remove motion artifact in resting state fmri. *NeuroImage* **84**(Supplement C), 320–341.
- TUSTISON, N. J., AVANTS, B. B., COOK, P. A., ZHENG, Y., EGAN, A., YUSHKEVICH, P. A. AND GEE, J. C. (2010). N4itk: Improved n3 bias correction. *IEEE Transactions on Medical Imaging* **29**(6), 1310–1320.
- VAN DER LAAN, MARK J, ROSE, SHERRI, ZHENG, WENJING AND VAN DER LAAN, MARK J. (2011). Cross-validated targeted minimum-loss-based estimation. *Targeted learning: causal inference for observational and experimental data*, 459–474.

VAN DER VAART, AAD W, WELLNER, JON A, VAN DER VAART, AAD W AND WELLNER, JON A. (1996). *Weak convergence*. Springer.

ZHANG, Y., BRADY, M. AND SMITH, S. (2001). Segmentation of brain MR images through a hidden markov random field model and the expectation-maximization algorithm. *IEEE Transactions on Medical Imaging* **20**(1), 45–57.